Engineering Failure Analysis 144 (2023) 106955

Contents lists available at ScienceDirect

Engineering Failure Analysis

journal homepage: www.elsevier.com/locate/engfailanal

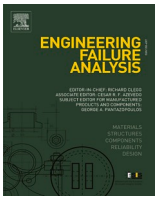

Crevice corrosion on stainless steels in oil and gas industry: A review of techniques for evaluation, critical environmental factors and dissolved oxygen

Eleani Maria Costa *, Berenice Anina Dedavid, Carlos Alexandre Santos, Natália Feijó Lopes, Caroline Fraccaro, Theo Pagartanidis, Lucca Piazza Lovatto

School of Technology, Pontifical Catholic University of Rio Grande do Sul, 6681 Ipiranga Avenue, Building 30, Room 111/F, 90619-900 Porto Alegre, RS, Brazil

ARTICLE INFO

Keywords:
Oil and gas engineering
Crevice corrosion
Stainless steel
Corrosion testing
Corrosion
Maintenance error
Dissolved oxygen

ABSTRACT

Crevice corrosion is a localized accelerated dissolution of metal that occurs as a result of a breakdown of the protective passive film on the metal surface. This work provides an overview from the literature of the most important techniques used for evaluating crevice corrosion and the critical factors influencing the crevice corrosion of stainless steels with emphasis to oil and gas industry. The phenomenology and mechanisms of crevice corrosion are discussed, including the effects of the alloy composition, environment, temperature, and dissolved oxygen on the corrosion behavior. Future development axes for studying crevice corrosion are proposed.

1. Introduction

Crevice corrosion is a type of localized corrosion that occurs in occluded regions of materials in contact with a stagnant corrosive fluid. The chemical reaction is caused by the presence of corrosive substances (corrodents) on the surface of a metal. The clogged area develops an extremely aggressive chemistry, forming a local composition, which promotes metal dissolution inside the crevice. Electrochemical potential differences result in selective crevice or pitting corrosion attack. Crevices can be formed between two metals or between a metal and a non-metallic surface [1,2]. Crevice corrosion and pitting corrosion are very similar, and generally occur in the presence of halide ions, typically chloride. Crevice corrosion usually begins with formation of pits. The main difference between crevice and pitting corrosion is that crevice corrosion requires a physical occluded region to develop. The presence of occluded regions is frequent in many engineering structures such as joints, flanges, metal surfaces under coatings, and environmentally assisted cracks in metallic materials [2–6]. It is problematic to prevent crevice corrosion since eliminating the electrolyte from the occluded regions is difficult.

Corrosion resistant alloys (CRAs) are susceptible to localized corrosion, as crevice corrosion. The initiation of crevice corrosion leading to the breakdown of the passive film in localized areas on CRAs is a consequence of a number of factors, including environmental, metallurgical, electrochemical and geometrical parameters [7,8]. The understanding of both mechanisms of passive film formation and breakdown can help in achieving better material selection for specific applications and corrosion prevention of CRAs. Among all environmental factors, the dissolved oxygen (DO) in the medium has a significant effect on the crevice corrosive process. In

* Corresponding author.
E-mail addresses: eleani@pucrs.br (E.M. Costa), carlos.santos@pucrs.br (C.A. Santos), natalia.feijo@pucrs.br (N.F. Lopes).

https://doi.org/10.1016/j.engfailanal.2022.106955
Received 27 July 2022; Received in revised form 10 November 2022; Accepted 20 November 2022
Available online 25 November 2022

such manner, it is important to understand the CRAs behavior depending on the DO content. The limit of oxygen in produced water and seawater systems for stainless steel usually used in oil and gas processes is 10 ppb for produced water systems and 20 ppb for seawater systems [9]. However, the maximum tolerable dissolved oxygen content to safely operate CRAs is uncertain, since there are several other parameters that should be taken into consideration, such as chemical composition, steel microstructure, concentration of chloride ions, and temperature [10–13]. The establishment of oxygen limits are of fundamental importance since higher oxygen limits for CRAs would bring not only economic benefits but will also improve the operations safety by a more accurate material selection. Currently, three main strategies are used in the oil and gas processes to prevent localized corrosion caused by oxygen. Investments in oxygen removal technologies, such as the use of oxygen scavengers, or specific *topside* facilities, or improvements in the current facilities with higher corrosion resistant materials [1,5,14,15]. Therefore, it is of great importance to concentrate efforts on the development of more effective methods of dissolved oxygen control and crevice corrosion evaluation and prediction which could permit the investigation and possible use of more cost-effective materials.

Despite all studies involving other forms of localized corrosion, there is no conclusive understanding of the processes occurring during the onset of CRAs crevice corrosion. The studies about crevice corrosion are mostly dedicated to stainless steels, as they are widely used in industrial manufacturing, transporting and construction [16–19]. Other systems susceptible to crevice corrosion are nickel alloys, aluminum alloys, and titanium alloys [7]. To mitigate the risk of localized corrosion in oil and gas processes, it is important to identify and understand the mechanisms and factors that control the initiation and propagation of this type of corrosion. The literature is abundant on pitting corrosion, but information related to crevice corrosion investigation is more limited and divergent on the relationship between material characteristics, environmental conditions, and crevice corrosion mechanisms in high-chromium stainless steels, mainly those used in the oil and gas industry. In addition, scarce and not recent review articles associated with crevice corrosion are available [7,20–22]. The aim of the current work is to present a literature review on CRAs crevice corrosion identifying

(a)

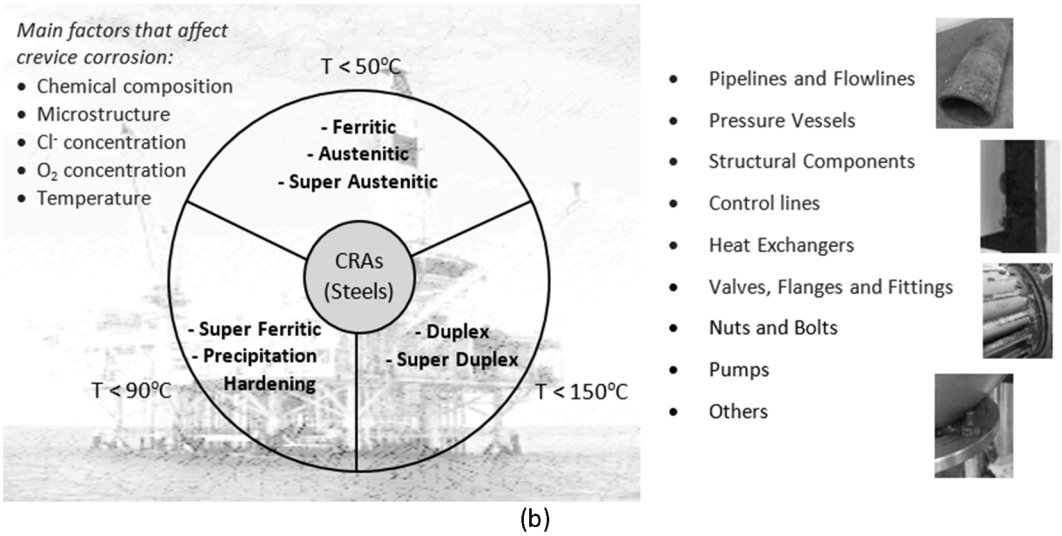

(b)

Fig. 1. (a) Oil and gas pipeline under crevice corrosion attack [17], (b) examples of CRAs and critical components for crevice corrosion.

what is already known and what needs to be further investigated in this field, with a particular emphasis on the main techniques for crevice corrosion evaluation, critical environmental factors, and dissolved oxygen limits, focusing on stainless steels.

2. Crevice corrosion in CRAs in the petroleum industry

Corrosion has an important economic and environmental impact. NACE International released the "International Measures of Prevention, Application and Economics of Corrosion Technology (IMPACT)" study in 2016, which estimated the global cost of corrosion to be approximately US$ 2.5 trillion. The report reviewed cost of corrosion studies performed by several countries and the annual corrosion costs ranged from approximately 1–5 % of their gross national product (GNP). Corrosion experienced in oil and gas production involves direct and indirect costs related to time, repair and/or replacement of materials, involvement of personnel in corrosion management, and safety and environmental consequences. The biggest threat to the integrity of oil and gas facilities is corrosion and fatigue [1,18,23–27].

Localized corrosion of CRAs in oil and gas infrastructures is challenging and difficult to mitigate due to its dynamic behavior, resulting not only in economic losses but also causing severe environmental damages [5,14,28]. There are several types of localized corrosion including pitting corrosion, crevice corrosion, intergranular corrosion, and exfoliation corrosion. Localized corrosion corresponds to an accelerated degradation of the metal at sites where the passive film has been compromised. The breakdown of the passive film, which leads to localized corrosion, is a challenging phenomenon, because it occurs on a small scale and during a short period, and its detection is difficult through regular inspection methods. This process is very dynamic and stochastic in nature. It is also affected by the heterogeneities of the metal surface, concentration gradients and the changing potentials [5,29].

Crevice corrosion is a common corrosion failure of CRAs and is considered even more dangerous than pitting corrosion since it occurs in occluded regions, which are in general not accessible and not visible. Much metal loss in oilfield casings and pipelines is caused by crevice corrosion [30,31] because of the creation of crevice due to welding, for example. Fig. 1a shows an oil and gas pipeline under crevice corrosion, while Fig. 1b presents examples of CRA steels, locations, and components where crevice corrosion is critical in the oil and gas industry. As illustrated in the schematic of Fig. 1b, the main metallurgical aspects that affect crevice corrosion resistance in high-chromium stainless steels are chemical composition and microstructure, while the most important environmental factors are temperature, chloride, and oxygen concentrations, as well as component or assembly configuration.

The crevice corrosion is mainly found in oxygen-containing systems and is intensified by the presence of aggressive ions, typically chloride. This type of corrosion often occurs in drill pipe joints, tubing or casing collars. The gap in the joint becomes devoid of oxygen and anodic. In the presence of salt water, the corrosion is promoted by the migration of negatively charged chloride ions to the crevice. Those ions not only counteract the buildup of positive charges around the crevice, but also act as a catalyst, accelerating the dissolution of the metal. This progressive process results in a deep pit [32]. Furthermore, in the coexistence of crevice and stress, the enhanced anodic reaction by applied stress accelerates the accumulation of H^+ and Cl^- ions within the crevice, which reduces the induction period and promotes the propagation of crevice corrosion [17].

At the beginning of their production life, oil and gas wells can be dry or produce a limited amount of formation water. Usually, the water cut (the ratio of produced water in a well compared to the total rate of produced fluids) increases with time as the well matures, and consequently the damage due to corrosion attack are susceptible to increase. Oxygen plays an important role in localized corrosion and is usually not present in formation water. However, in the drilling stage oxygen-contaminated fluids are introduced, and this oxygen dissolved in drilling fluid promotes crevice and pitting attack of metal in the shielded areas of drill string. That is the common cause of failures and destruction under rubber pipe protectors. Another typical source of oxygen is the injection of water into producing fields to maintain reservoir pressure and/or for water flooding purposes. This water may come from a variety of sources including produced water, treated water and seawater. Therefore, an important aspect of materials selection for water injection wells is the crevice corrosion resistance of CRAs. This corrosion issue is particularly relevant for cases where injection water is a mix of different water types. In such cases, dissolved oxygen is not fully controlled or removed and, in some situations, fully oxygenated water may be injected [9]. Tubular connection threads used for well construction are known crevice formers. Therefore, the presence of crevices in well tubing is assumed, and the susceptibility to crevice corrosion shall be assessed as part of the materials selection process for water disposal and injection wells [9].

In oil and gas topside applications, pitting and crevice corrosion at temperatures above 50 °C and stress corrosion cracking (SCC) are the most common types of corrosion attack [30]. When crevices are present, crevice corrosion generally initiates under less severe conditions of chloride, oxygen and temperature compared to pitting corrosion. Although a number of studies were conducted to understand pitting corrosion and crevice corrosion, the effect of environmental factors on these types of corrosion is not fully understood, as discussed in section 5 of this article. Nevertheless, the literature is scarce regarding localized corrosion in offshore environments, which can be related to the lack of measuring methods and the difficulties in controlling the environment [18]. Therefore, more experimental data and methods, as well as computational models, are required to explain and predict the location, time and severity of localized corrosion, including crevice corrosion under real operating conditions.

3. Crevice corrosion mechanisms

Considering a typical metal in a medium containing chloride ions as produced water or seawater, the general mechanism of crevice corrosion involves initially anodic reactions (metal oxidation) followed by cathodic reactions (oxygen reduction), both taking homogeneously place at the metal surface inside and outside the crevice. The electrons originating from the oxidation are consumed in the oxygen reduction reaction, hence, one hydroxyl ion is formed for each metallic ion in the solution. Due to non-renewal of the

electrolyte and chlorides ions accumulation, the amount of oxygen declines in the occluded area as a function of time, and consequently, the reduction reaction starts to develop more on the outside crevice area (open area). The metal dissolution, however, continues to occur, causing an excessive number of positive charges within the crevice. In order to maintain electroneutrality, chloride ions migrate to the inner part of the crevice. In general, crevice corrosion happens in three stages: incubation, initiation and propagation [7]. There are valuable book chapters on crevice corrosion [2] where fundamental concepts are presented, and relevant information are offered and discussed.

Stainless steels are susceptible to crevice corrosion because the chromium oxide film (which serves as a barrier against corrosion) is attacked by corrosive ions (typically chlorides), increasing metal dissolution. Correspondingly, the decrease in pH inside the crevice accelerates corrosion, since present H^+ ions create gaps in this passive film (chromium oxide), exposing the base metal. The pH value below which the integrity of the passive film cannot be maintained is called depassivation pH. Crevice corrosion of stainless steels is an extremely complex process that can be described using different models. Although other models exist, such as metastable pits and dissolution of inclusions, this work focuses on Critical Crevice Solution (CCS) and IR drop theories.

The CCS theory, also called acidification model [33] is the model where crevice corrosion is explained by a pre-existing passive oxide dissolution that depends on the solution acidification of the crevice, caused by chloride ion migration to this area, as a result of dissolved oxygen depletion. In the initial induction period of crevice corrosion, uniform metal dissolution occurs both inside and outside of the crevice [34]. Fig. 2 shows a schematic representation of the crevice corrosion mechanism detailing the main electrochemical reactions. The main anodic reaction is given in reaction (1), and the possible cathodic reactions are oxygen reduction and/or hydrogen evolution reaction, given by reactions (2) and (3), respectively.

$$M \rightarrow M^{n+} + ne^- \tag{1}$$

where M represents the metal and Mn^+ represents the metal ions.
The possible cathodic reactions are:

$$O_2 + 2H_2O + 4\,e^- \rightarrow 4OH^- \,(oxygen\ reduction\ reaction\ -\ ORR) \tag{2}$$

$$2H^+ + 2\,e^- \rightarrow H_2\,(hydrogen\ evolution\ reaction\ -\ HER) \tag{3}$$

The extra positively-charged metallic ions are electrostatically counter balanced by migration of negatively-charged ions such as Cl^- and OH^- from the bulk solution to the inner part of the crevice. After the oxygen in the crevice becomes depleted, the reduction of oxygen continues in the outer surface, and the metal dissolution reaction may still occur in the crevice, leading to both the separation of anodic and cathodic reactions and the net anodic metal dissolution. Metal ion hydrolysis and electromigration increase the H^+ and Cl^- concentration in the crevice, and can be expressed by the following reactions:

$$M^{n+} + nCl^- \rightarrow MCl_n \tag{4}$$

$$MCl_n + nH_2O \rightarrow M(OH)_n + nH^+ + nCl^- \tag{5}$$

$$M^{n+} + nH_2O \rightarrow M(OH)_n + nH^+ \tag{6}$$

H^+ and Cl^- in the crevice electrolyte attack and destroy the passive film on crevice wall, switching crevice wall from passive state to active state. Thus, metal dissolution in the crevice is accelerated by the autocatalytic reactions and the propagation stage of crevice

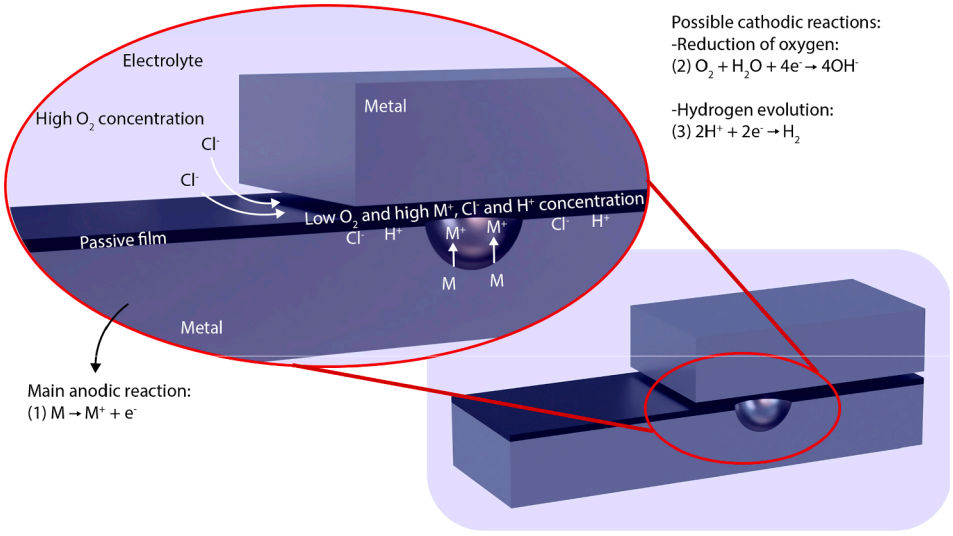

Fig. 2. Crevice corrosion illustration and main electrochemical reactions.

corrosion starts.

The CCS model is principally dependent by the manner in which the occluded geometry of a crevice restricts the mass transport of species (diffusion and migration only) into and out of the occluded region, resulting in a crevice solution chemistry that is different from the bulk solution. This model predicts that the highest corrosion rates within the crevice must occur at the deepest region of the crevice. The main disadvantage of this model is it assumes that the passive current density is low enough to not result in an appreciable potential drop within the crevice, partially ignoring the potential dependence of corrosion rate. However, the current flowing through the crevice increases by orders-of-magnitude after crevice corrosion initiates, invalidating this assumption [2]. Therefore, the main limitation of CCS model is that it is not predictive for crevice corrosion propagation rates. In addition, it cannot predict the occurrence of intermediate attacks, which are the most common form of crevice corrosion damage distribution [2,34]. As a consequence, recent mathematical models (so called transient models) based on the acidification model have been developed to predict the initiation and propagation rate of crevice corrosion [29,35,36].

The second model is IR drop Theory (mostly ruled by crevice geometry) which is defined by a drop in ohmic potential values in the crevice area, turning it into an active–passive transition [37]. At locations where the potential drops to a critical value, defined as E_{pass} (also referred to as E_{crit}), the current density increases considerably as the passive film is no longer stable, leading to active dissolution (Fig. 3) [2]. The IR drop mechanism has been receiving more attention because this mechanism provides an understanding for corrosion processes in both chloride-containing and chloride-free environments, unlike the CCS model. However, the IR drop model is more applicable to metal/electrolyte systems which exhibit active/passive behavior in the solution within the crevice [2,22]. Efforts have been attempted to combine CCS and IR drop mechanisms in order to accurately predict crevice corrosion in many alloy/electrolyte systems, as is the case of CRA steels, and its advantages and limitations were discussed by Kelly & Lee [2] and Kennell et al. [22]. The mathematical model proposed by Kennell et al. [22], that combines CCS and IR, showed good agreement with the experimental data. Three crevice corrosion phases were determined corresponding to the evolution of electrical potential drop within the crevice: total corrosion phase, the dynamic phase, and the quasi steady-state phase.

Both theories agree on the oxygen depletion within the crevice. Therefore, the dissolved oxygen (DO) concentration within the crevice solution is one of the most important factors that affects the crevice corrosion behavior. Oxygen is a strong oxidant with relatively fast reduction kinetics. Moreover, oxygen has a rather low solubility in water and brines, and this explains why mass transport of oxygen is the rate-limiting step in the corrosion reactions of steels in non-acidic environments [14]. This also elucidates the localized attacks in crevices and under deposits that are attributed to the limited mass transport in oxygenated systems. In general, the concentration of dissolved oxygen is between 7 and 8 ppm at ambient equilibrium conditions between air and water. The corrosion rate for low alloyed steels at this concentration and under stagnant conditions is about 0.25 mm/yr (10 mpy). Under higher turbulent flow conditions, it could reach values as high as 150 mm/yr (6000 mpy), assuming continuous oxygen replenishment. By scavenging oxygen to 7–8 ppb, the corrosion rate can be reduced to $<$0.01 mm/yr (0.4 mpy) [14]. The chemical composition and microstructure of the corrosion resistant steels are important factors that influence crevice corrosion rate as discussed in section 5.2 of this article. As a consequence of this complex synergy, several works are discrepant regarding the safe level of dissolved oxygen when CRA steels are used. In addition, different behaviors were observed in real operations and laboratory simulations, which encourages further studies and discussion, which is the reason of the present work.

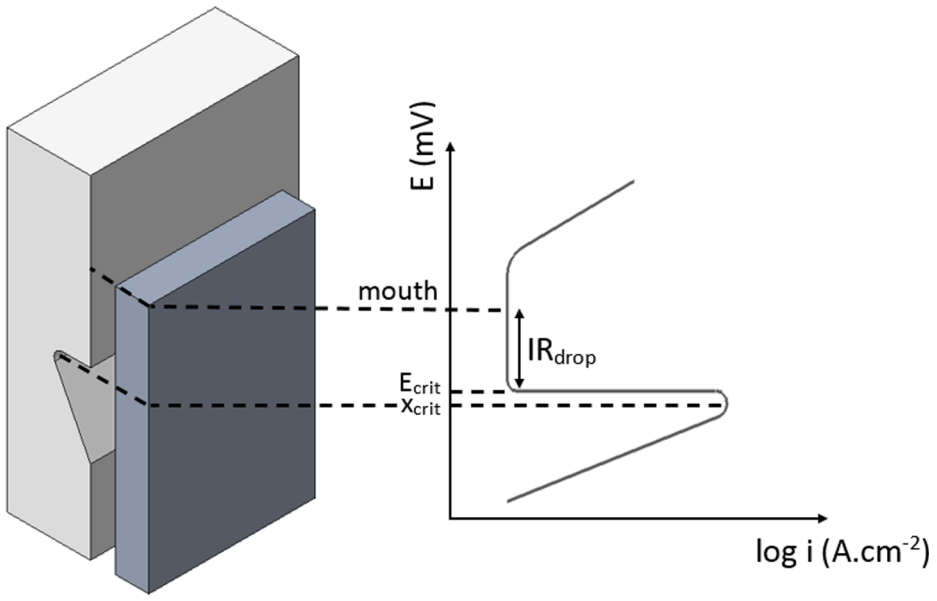

Fig. 3. IR drop model which focuses on how the restricted geometry causes potential drops in the solution within the occluded site. (). adapted from [2]

4. Techniques for crevice corrosion evaluation

There is a relatively large number of acknowledged test methods to study and quantify crevice corrosion. The different methodologies have been used for comparing and ranking alloys and for quality control, assessing the effects of manufacturing route and alloy composition changes on crevice corrosion resistance, as well as to determine critical temperatures and electrochemical potentials [2,38,39].

Methods for determining the crevice corrosion resistance are often divided into three categories: (1) nonelectrochemical or immersion, (2) electrochemical at open circuit potential with no applied signal, and (3) electrochemical with applied signal (with polarization) [2]. Is it important to note that the use of each test method and their acceptance criteria vary between the different oil companies [40].

4.1. Nonelectrochemical or immersion methods

The ASTM G48 standard test method [41] provides procedure details for testing crevice and pitting corrosion resistance of stainless steel alloys. Test Methods B, D, and F are used to evaluate crevice corrosion where artificial crevices are formed on metallic specimens of the selected alloy with nonmetal crevice formers. Method B specifies 6 wt% ferric chloride ($FeCl_3$) as the oxidizing and corrosive electrolyte to produce localized corrosion under the crevice formers. Temperature is maintained at 22 or 50 °C with an exposure time of 72 h. Crevice corrosion resistance is evaluated by mass-loss, maximum penetration depth, and attack area. Methods D for nickel-based and high chromium alloys and method F for stainless alloys use acidified ferric chloride solution to determine the critical crevice temperature (CCT). Multiple crevice assemblies are used as crevice formers with the purpose to increased statistical analysis (Fig. 4). The ASTM G48-A test (ferric chloride test) is also widely used for pre-qualification of welds and weld overlays of CRAs within the oil and gas industry. Mathiesen & Andersen [40] published a study about potential problems associated with the ASTM G48 testing for prequalification of base metals, weld and overlay welds of CRAs. The authors discussed several aspects such as coupon cutting and preparation, cut-face pitting, pit identification, exposure time, and influence of test temperature. However, the focus of the study was in pitting corrosion of CRAs. Final finish of the cut faces is less important as long as polishing is done wet. Possible pitting on cut faces is more dependent on a pickling treatment, which can dissolve discovered slag particles that otherwise could initiate pitting. ASTM G78 standard guide [42] is similar to ASTM G48 with the exception that seawater is used as the chloride-containing electrolyte, whereas the ISO 18,070 test [43] specifies corrosion formers with disc springs for crevice corrosion testing of flat or tubular specimens. However, this standard specifies no information related to the procedures for crevice corrosion testing and evaluation of attack. The crevice

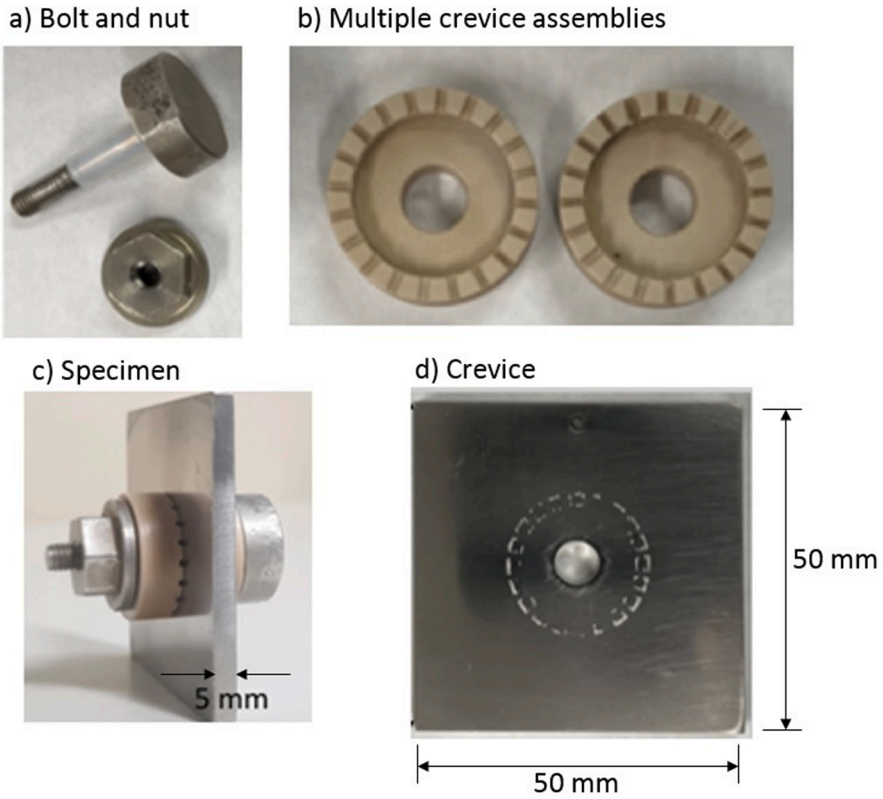

Fig. 4. Example of multiple crevice assembly based on the ASTM G48 standard test method.

former can be easily adapted for electrochemical measurements.

4.2. Electrochemical methods

There are several aspects to take into consideration when studying crevice corrosion of CRAs. For a better understanding of the influence of environmental factors involved and to fill potential knowledge gaps, electrochemical studies are necessary. Electrochemical techniques used to assess crevice corrosion include techniques where no external signal is applied (open circuit) and those that involve the disturbing the system with an applied signal (polarization). Some of these techniques are discussed below.

4.2.1. Electrochemical methods at open circuit

In this category, the corrosion potential (E_{corr}) of a crevice exposed to an electrolyte is measured against a reference electrode at open circuit. This technique is the most basic electrochemical measurement, and its main advantage relies on the use of signal techniques that mimic what happens in real systems where crevice corrosion can initiate, propagate, and repassivate. The abrupt decrease in E_{corr} often indicates active crevice corrosion, but knowledge of the metal/electrolyte system is required for an accurate interpretation of results. However, no information regarding reaction rate can be determined using open-circuit measurements since current does not flow between the crevice and the reference electrode. Open circuit measurements can be combined with ASTM G48 Standard to provide transient E_{corr} measurements during evaluation of crevice corrosion [2].

Current flow during crevice corrosion at open circuit can be measured using a remote crevice assembly and following galvanic corrosion testing guidance of ASTM G71[44] standard test method. Anode (creviced) and cathode (non-creviced) are connected through a zero-resistance ammeter (ZRA) and the current (and potential if using a reference electrode) are monitored. The initiation of crevice corrosion is associated with a sharp increase in current. Attention must be taken in the geometric design of the remote crevice assembly including the anode/cathode surface ratio. The remote crevice assemblies often can underestimate metal loss during open-circuit testing [2].

4.2.2. Electrochemical methods with applied signal

Perturbation of the system by application of an external signal in the form of a voltage or a current (against a counter electrode) provides information in terms of both system potential and reaction rates. When the applied signal is a constant voltage, the technique is referred to as potentiostatic. This method is widely used in the study of crevice corrosion. Holding the voltage of a system potentiostatically provides the current as a function of exposure time. The advantage of the potentiostatic method is that it is easy to set-up, and interpretation of the resulting current can provide information on crevice initiation and propagation, with increase in current often indicates the onset of active crevice corrosion. The disadvantage of this method is that it can provide cathodic currents (against a counter electrode) higher than a local cathode could supply. Therefore, rates of reaction are often overestimated in comparison to

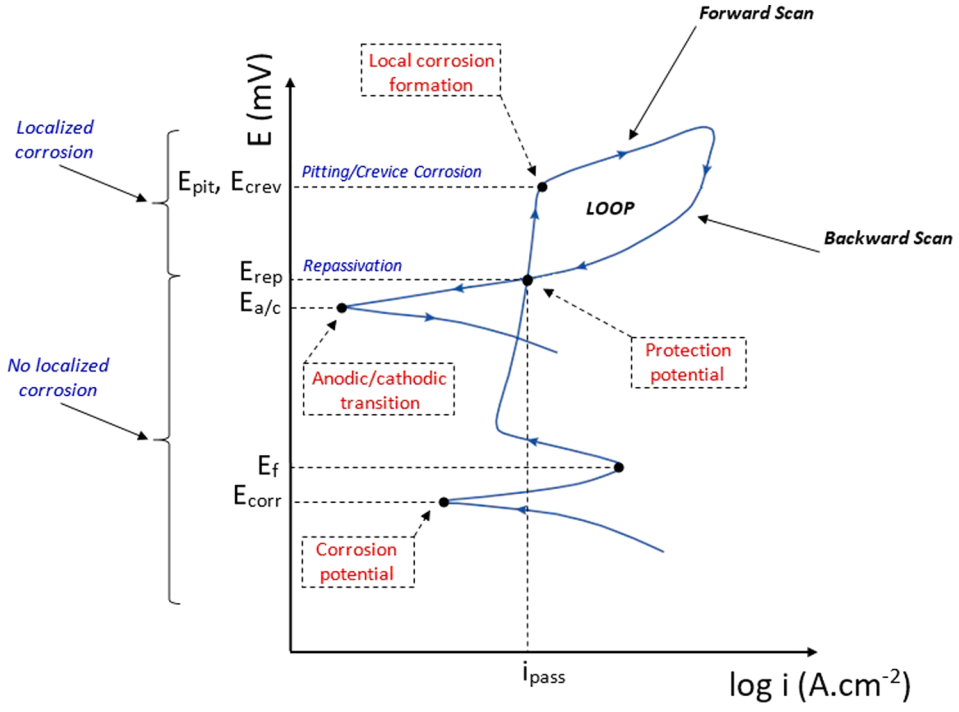

Fig. 5. Cyclic potentiodynamic polarization (CPP) ().
adapted from [46]

open-circuit exposures limited by the anodic or cathodic reactions [2].

Cyclic potentiodynamic polarization (CPP) is the most widely used technique to evaluate critical crevice corrosion potentials [2,12,19,45]. Through this technique, pitting or crevice potentials (E_{pit}, E_{crev}), repassivation potential (E_{rep}) and corrosion potential (E_{corr}) can be determined, as illustrated in Fig. 5. The CPP technique consists in a slow potentiodynamic polarization scan up to a target current density value. The current density value must be high enough to initiate localized corrosion during the forward scan. As soon as the target current density value is reached, the direction of the polarization is reverted during the backward potentiodynamic polarization. Crevice potential (E_{crev}) is determined at the inflection point corresponding to a sharp increase in anodic current of the forward scan. Repassivation potential (E_{rep}) is defined as either a cross-over potential or when the backward scan reaches the passive current density (i_{pass}) [2,45,46]. More information about interpretation of CPP test results for study of corrosion behavior of metals can be found in Esmailzadeh et al. [46]. The ASTM G61[47] standard is a test method for conducting CPP measurements for localized corrosion susceptibility of iron-, nickel-, or cobalt-based alloys. This test method was designed to investigate the susceptibility of local corrosion, such as pitting and crevice corrosion in a chloride environment. The ISO 15,158 standard test method [48] is a fast method that also can be considered for evaluation of crevice corrosion. This standard describes the procedure for determining the pitting potential for stainless steels under potentiodynamic control. The pitting or crevice potential can be measured in a single potential scan and can be applied to compare the relative performances for different stainless-steel grades.

The E_{crev} can be determined with good reproducibility though CPP technique, but E_{rep} are not highly reproducible particularly when the alloy is not very susceptible to crevice corrosion or when the environment is not highly aggressive. The E_{rep} dependence with the extent of pit and crevice propagation can be related to the electrical charge passed during the forward scan [46; 52]. For some CRAs, for example UNS S30400 (AISI 304) and UNS S31603 (AISI 316L) austenitic alloys, and UNS N08825 (AISI Alloy 825) austenitic nickel–iron-chromium alloy, E_{rep} becomes independent from the degree of the attack when the propagation is deep enough (electrical charge > 10–30C/cm^2) [52]. Thus, the existence of a minimum pit or crevice depth is necessary to obtain reproducible E_{rep} values. Besides, especially for highly alloyed CRAs, the CPP method might allow insufficient time for localized corrosion propagation during the forward scan, whereas the backward potentiodynamic scan starts as soon as the pre-defined current density is reached [2]. Alternative methods to avoid the limitations of the CPP technique were developed and reported in the literature [45,49]. For example, Tsujikawa & Hisamatsu~~, 1980~~ [50]~~,~~ developed an electrochemical test to study crevice corrosion of nickel-based CRAs, which is referred to as the Tsujikawa-Hisamatsu Electrochemical (THE) method. This multi-step technique was standardized in the ASTM G192 [51] standard and consists of the following steps: (i) potentiodynamic polarization (PD) to a potential more positive than critical potential, (ii) galvanostatic polarization (GS) for 2 h to let localized corrosion propagates, and (iii) iterative potentiostatic polarization (PS), lowering the potential 10 mV every 2 h until repassivation is achieved. Due to the GS step, the total charge passed is better controlled as the current is held constant during the time of the galvanostatic step [2,45]. The main advantages of this method (also known as PD-GS-PS method) are that localized corrosion is controlled by galvanostatic polarization for fixed charged density and the repassivation potential is determined by monitoring current decrease at each potentiostatic step [52]. As a result, a sufficiently deep localized attack can develop, leading to more reproducible E_{Rep} values. E_{Rep} is defined in this technique as the highest potential where the current stops increasing during the PS. Nevertheless, the THE method is slow and time consuming as E_{Rep} is usually found at low potentials. Thus, it often takes many iterations and a long time to reach E_{rep} using 10 mV steps every 2 h. Additionally, in some cases, it is difficult to discern when repassivation occurs due to the current behavior during the PS step, complicating the determination of E_{Rep} [2,45].

Mishra & Frankel [53]changed the third step of the THE test to a backward PD scan. As for CPP, E_{Rep} is defined as the cross-over of both potentiodynamic scans or when the backward scan reaches i_{pass}. This technique was referred to as the PD-GS-PD method by the authors, named to reflect the three different steps, specifically: (i) potentiodynamic polarization scan (PD), (ii) galvanostatic polarization (GS), and (iii) reverse potentiodynamic polarization scan (PD). Thereby, the issues mentioned above with the CPP and the THE techniques were resolved. In a PD-GS-PD scan, crevice corrosion develops during the GS step, resulting in a low scatter of the results while keeping the testing time short [2,45]. Typical results from PD-GS-PS and PD-GS-PD methods are shown in Fig. 6.

The PD-GS-PD has been applied to the analysis of localized corrosion resistance of nickel-based alloys [54,55] but is less used to test

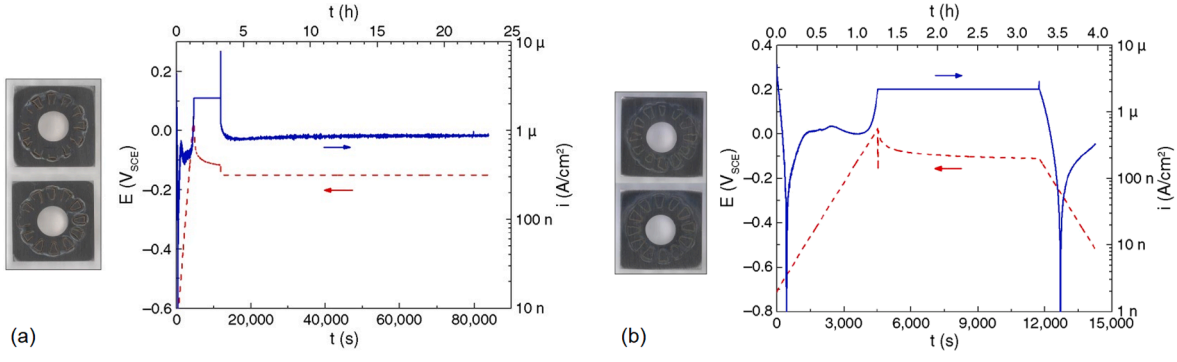

Fig. 6. (a) PD-GS-PS and (b) PD-GS-PD tests for UNS N06022 (AISI Alloy 22) in deaerated pH 6, 1 M NaCl at 90 °C ().
adapted from [54]

conventional and highly-alloyed stainless steels [56]. Results showed that the PD-GS-PD method presented the most conservative crevice repassivation potential (E_{rep}) values among the different methods, i.e., the lowest values in comparison to the CPP and THE tests. In addition, these E_{rep} values were independent of the scan rate used during the PD steps [53], torque applied to the crevice former (if>2 N.m) [55], and the charge passed during the GS step [54]. Torres et al. [46] also detailed some additional disadvantages of using this technique to evaluate crevice corrosion of super duplex stainless steel at temperatures ranging from 22 to 60 °C, such as the effect of the metastable activity and high current noise that was high enough to trigger the GS step before reaching the critical crevice potential, and the forward scan can reach transpassive values, which could influence the crevice initiation.

Wu et al.[56], investigated crevice corrosion performances of a newly developed lean duplex stainless steel (LDSS) AISI 2002 alloy (21.1Cr-3.2Mn-1.8Ni-0.16 N-0.4Mo) and three commercial alloys (AISI 304 and AISI 316L austenitic stainless steels and AISI 2205 duplex stainless steel - DSS) by the PD-GS-PD measurement techniques. The applicability of E_{rep} and E_{crev} in crevice corrosion evaluation of these four austenitic and duplex stainless steels was discussed. Crevice repassivation potential was applicable to crevice corrosion evaluation of AISI 304 and AISI 316L stainless steels. However, much lower E_{rep} values were obtained for AISI 2205 (duplex) and AISI 2002 (lean duplex). These anomalous E_{rep} values for duplex stainless steels may be related to the selective attack of the less corrosion-resistant phase, the lower corrosion potential in the crevice-like solution, and more crevice corrosion initiation sites in the PD-GS-PD test. A critical chloride concentration of crevice corrosion (CCC_{Crev}) measurement was introduced for crevice corrosion evaluation of various stainless steels. The derived CCC_{Crev} was assessed to be a valid criterion for crevice corrosion evaluation of both the austenitic and duplex stainless steels. An order of crevice corrosion resistance of AISI 304 ≈ AISI 2002 (LDSS) < AISI 316L < AISI 2205 (DSS) was suggested, which agrees with the orders of pitting resistance equivalent number (PREN) and critical crevice index of the less corrosion-resistant phase in each material.

Application of a constant current to the system is referred to as the galvanostatic method. This method is used less frequently in the study of crevice corrosion but can be used due to its similarity with open-circuit conditions where the cathodic current is limited by the cathode size. The main disadvantage of the galvanostatic method is that constant current is required to provide marginal information regarding reaction rates [2].

The critical crevice temperature and critical repassivation temperature (CRT) are also valid criteria for determining the crevice corrosion susceptibility of stainless steels [57,58]. The ATSM G150 [59] standard is a test method for evaluating the resistance of stainless steel and related alloys to pitting corrosion. The method is based on the determination of the critical pitting corrosion temperature (CPT) by the potentiostatic technique using a temperature scan. The procedure can be adapted to determine CCT. The specimen is exposed to a 1 M NaCl solution, initially at 0 °C. After an initial temperature stabilization period, the solution is heated at a rate of 1 °C/min. About 60 s before the temperature scan is achieved, the specimen is anodically polarized to a potential above the pitting potential range. This potential is held constant during the whole temperature scan. A potential of 700 mV versus SCE (25 °C) has been found suitable for the most common stainless steels. The current is monitored during the temperature scan, and the CPT is defined as the temperature from which the current increases rapidly, defined as the temperature at which the current density exceeds 100 μA/cm^2 for 60 s.

The CCT and CRT can also be determined by CPP or PD-GS-PD techniques by testing a selected alloy at different temperatures. However, Han et al.[57] investigated the CCTs of UNS S32101 (AISI 2101), UNS S31803 (AISI 2205), and UNS S32750 (AISI 2507) duplex stainless steels in chloride solutions and a CCT value of 2 °C was determined for UNS S32101. Then CCTs of the lower-grade duplex stainless steels (DSSs) may be<0 °C, suggesting that CCT can be not applicable to low-grade stainless steels for crevice corrosion evaluation.

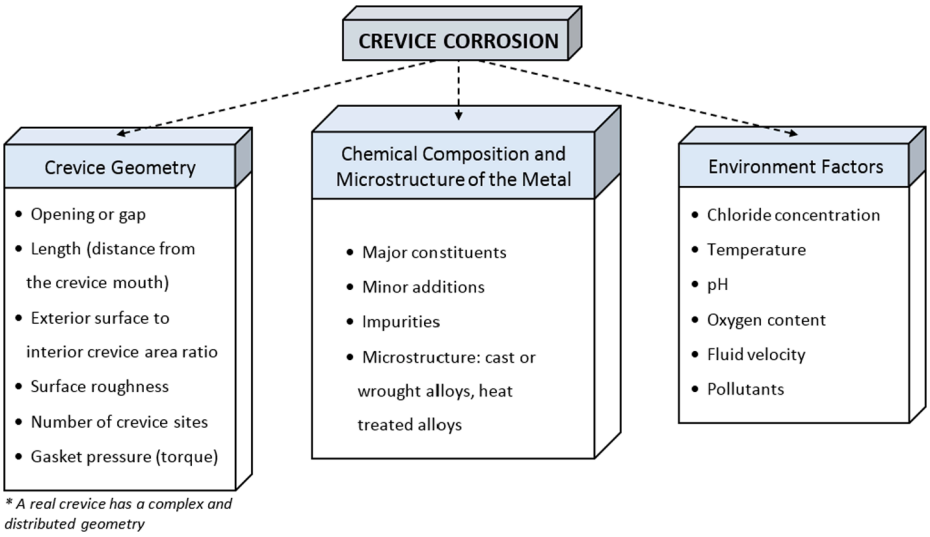

Fig. 7. Critical factors that influence on crevice corrosion ().
adapted from [7]

Other electrochemical techniques have been applied to evaluate crevice corrosion, such as linear potentiodynamic polarization (LPP) and dynamic electrochemical impedance spectroscopy (EIS). In the study of Nagarajan & Rajendran [60] the critical crevice potential measured from the polarization data was in good agreement with the dynamic electrochemical impedance spectroscopic data. The authors use the AFM (atomic force microscopy) technique to characterize the surface morphology of the pits after crevice corrosion tests. The use of EIS is a powerful technique to understand the effect of alloying element, structural defects, and others parameters on the passive film properties at critical potentials. However, relatively few studies have applied EIS to study crevice corrosion perhaps related to the main difficulty that the electrochemical system must remain in a stationary state during the measurement over the frequency range of interest.

5. Critical factors of crevice corrosion

The occurrence of crevice corrosion in CRAs depends on several factors related to the metal and the environment, such as [7]:
- Crevice geometry,
- Chemical composition and microstructure of the metal,
- Environmental factors: Chloride concentration, temperature, pH, fluid velocity, and oxygen content.

Factors influencing crevice corrosion are summarized in Fig. 7. The main critical factors influencing crevice corrosion of CRAs are detailed and discussed in the following sections.

5.1. Crevice geometry

A crevice is formed when two surfaces, at least one being metallic, are in close proximity and immersed in a corrosive electrolyte. Geometry affects more crevice corrosion compared to pitting corrosion. The crevice geometry is defined by the opening or gap (g) and the length (L) measured as the distance from the crevice mouth (Fig. 8), exterior surface to interior crevice area ratio, and number of crevice sites. The gap has to be wide enough to allow ingress of the bulk solution, but sufficiently tight to promote the formation of an occluded environment within the cavity. Openings (g) between 0.1 and 100 μm have been typically found to cause crevice corrosion. Crevice corrosion rarely occurs in wide gaps ($g > 3$ mm) [36,39]. The surface roughness can also impact crevice corrosion. The average CCT decreases with the increase in surface roughness. A real crevice has a complex and distributed geometry that cannot be defined rigorously, resulting in a wide range of crevice gaps, including areas of direct intimate contact.

Larché et al. [61] also found that critical CCTs in seawater were highly dependent on the crevice geometry defined by the roughness of the specimens and the gasket pressures. However, many types of crevice simulators made of different materials have been reported in literature, as a consequence comparison of results related to CRAs performance is challenging. Besides, the applied torque is another factor of influence on crevice corrosion. Different magnitude of load (torque) has been applied to ensure a tight crevice; but the size of the formed is often not measured. Another difficulty found in crevice corrosion tests is simulating crevices on non-flat surfaces and controlling the torque. Chang et al. [35] proposed an apparatus and a procedure to measure the initiation temperature of crevice corrosion in tubular shape products such as pipes, tubes and round rods. The test method was also found to be applicable to plate type specimens. The authors presented an equation used to calculate the applied torque for different diameters of cylindrical specimens valid for diameters above 15 mm.

Cai et al. [19] investigated the effects of applied torque on the crevice corrosion behavior of AISI 316L stainless steel using the CPP method. Three kinds of crevices (316L-to-polytetra-fluoroethylene, 316L-to-fluoroelastomeric and 316L-to-316L) were tested in artificial seawater at 50 °C, as illustrated in Fig. 9. Similar behaviors in crevice corrosion susceptibility with increasing applied torque

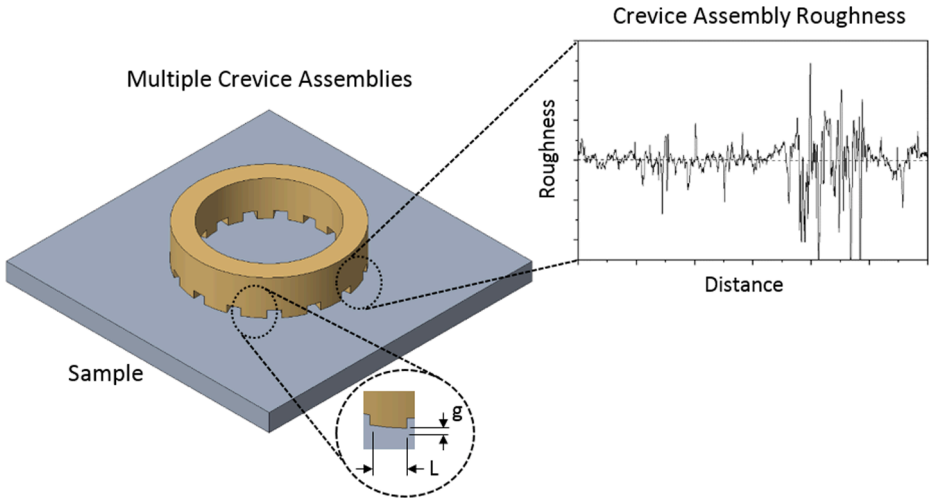

Fig. 8. Geometry of crevice corrosion.

were observed. The 316L stainless steel specimen coupled to the 316L stainless steel crevice former was the most susceptible to crevice corrosion.

Kim et al. [62] studied the effect of crevice former type on the corrosion behavior of AISI 316L (UNS S31603) stainless steel in a heat exchanger using electrochemical methods and surface analyses in chloride-containing synthetic tap water (60 °C). Two crevice types were used, namely metal–metal and metal-EPDM (ethylene propylene diene M−class). The metal-EPDM crevice was used to simulate the crevice under gasket, and the metal–metal to simulate the crevice between heat plates of the heat exchanger. The localized corrosion under metal–metal crevice conditions was initiated more easily than under the metal-gasket crevice conditions due to the restricted mass transport at the gasket crevice mouth. However, the anodic current under the metal–metal crevice conditions was lower than under metal-gasket crevice conditions at a higher anodic potential, indicating that the metal dissolution under EPDM crevice is higher than metal crevice under the accelerated corrosion condition. It was observed that the damage tendency under metal-gasket crevice condition is much higher than under metal–metal crevice conditions due to narrow crevice formed under gasket, accelerating the anodic dissolution at the crevice mouth. Based on the results, it is evident that expanding discussion on crevice corrosion under different conditions is essential to elucidate the involved mechanisms and improve the response of steels.

However, few studies have reported the effect of crevice geometry on crevice corrosion of metal at high temperature pressurized water due to difficulties in simulating such tests. Chen et al. [36] have developed an exposure testing device of crevice corrosion in high temperature pressurized water which can control the crevice geometry (Fig. 10a). They studied the effect of crevice geometry on the corrosion behavior of AISI 304 (UNS S30400) stainless steel in 290 °C water containing 3 ppm DO and investigated the structure, morphology and composition of oxide films within the crevice. Both crevice width and crevice length were determined to affect the oxidation behavior of AISI 304 stainless steel during crevice corrosion in high temperature pressurized water (Fig. 10b and c). Different crevice widths result in various distributions of DO within the crevice, and consequently in different potential drops. The results showed that crevice length has less effect on the DO distribution than the crevice width. The crevice length mainly influences the pH value within the crevice solution.

Since crevice corrosion is diverse and is difficult to be directly monitored, most investigations have to be performed using ex-situ methods, which can make the analysis of mechanisms challenging. Yang et al. [34] used a combination of in-situ and ex-situ techniques to study crevice corrosion of UNS S32101 using a transparent convex glass lens as crevice forming material. The convex glass lens in contact with a flat metal surface is presumably capable of providing infinite aspect ratio (crevice depth divided by its opening dimension). The relocation of active dissolution region on the crevice wall that contributed to the diversity of crevice corrosion morphology was explained by the effects of corrosion products based on the IR mechanism.

5.2. Metal chemical composition and microstructure

CRAs generally include a wide range of steels containing various alloying elements (as Cr, Ni, Mo, W), which tend to form a passive film. Table 1 shows the chemical compositions of the most important stainless steels.

The resistance of stainless steels to localized corrosion is a function of the thickness and composition of the passive film on the metal surface. Stainless steels exhibit a non-continuous and porous oxide film, usually 1–5 nm thick, which provides resistance to localized corrosion on the surface. This film gives a barrier to oxidation reaction at the metal surface due to their lower ionic conductivity. The passive film consists of two layers, an inner oxide layer and an outer hydroxide layer. The interaction of the passive film with an aqueous solution is responsible for the formation of the outer hydroxide layer, while the inner layer of the passive film contains oxides and hydroxides of the alloying elements present in the steel. The stability of the passive film formed on stainless steels is dependent on the alloy composition, temperature, and the exposure environment [64]. Therefore, chemical composition of metal and microstructure have important influence on crevice corrosion. As well known, there are many similarities between pitting and crevice corrosion, thus it can be assumed that alloying elements that affect pitting corrosion will also have some impact on crevice corrosion resistance.

In general, Cr, Mo, Ni and W contents increase the resistance to depassivation and improve localized corrosion resistance to chloride-containing electrolytes with a pH value ranging from slightly acidic to moderately alkaline [45,49,65–67]. Haugan [68] showed that W has a beneficial effect on localized crevice corrosion with an increase in CCT and CRT of 10 °C. Torres et al. [45] investigated the effect of W (0.0, 0.6, and 2.1 wt%) on critical temperatures of solution annealed 25Cr duplex stainless steels (UNS 32,750 UNS 32,760 and UNS 39274). The PD-GS-PD technique was used to estimate the critical crevice repassivation temperature by

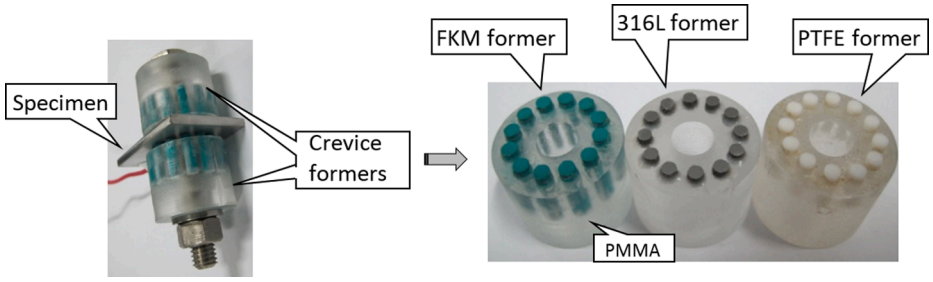

Fig. 9. Specimen assembled in the modified crevice former confectioned by PMMA and multiple cylinders of FKM, AISI 316L and PTFE (). adapted from [19]

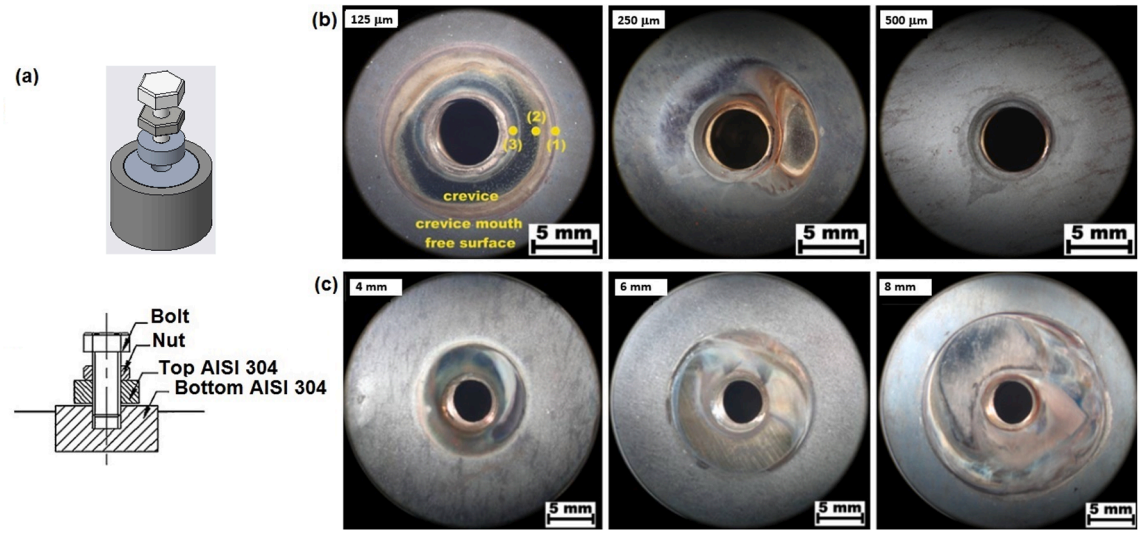

Fig. 10. (a) High temperature crevice corrosion device and images of surface corrosion after 150 h exposure tests in 290 °C water containing 3 ppm DO at different crevice (b) widths and (c) lengths ().
adapted from [36]

Table 1
Nominal chemical compositions of some CRAs steels used in the oil and gas industry [63].

Type	UNS	AISI	C	Mn	Si	Cr	Ni	Mo	N	Others
Austenitic	S30403	304L	≤ 0.03	2.0	1.0	18.0 – 20.0	8.0 – 12.0			
	S31600	316	≤ 0.08	2.0	1.0	16.0–18.0	10.0–14.0	2.0–3.0	≤ 0.11	
	S31603	316L	≤ 0.03	2.0	1.0	16.0–18.0	10.0–14.0	2.0–3.0	≤ 0.11	
Super austenitic	S31254	254 SMO	≤ 0.02	1.0	0.8	19.5–20.5	17.5–18.5	6.0–6.5	0.18–0.22	0.5–1.0 Cu
	S31266	S31266	≤ 0.03	2.0		23.0 – 25.0	21.0 – 24.0	5.2 – 6.2	0.35 – 0.6	1.0 – 2.5 Cu
Martensitic	S42000	420	0.15 min	1.0	1.0	12.0–14.0				
	S44004	440C	0.95–1.2	1.0	1.0	16.0–18.0		0.75		
Precipitation hardening	S17400	17–4 PH	0.07	1.0	1.0	15.5–17.5	3.0–5.0			3.0–5.0 Cu, 0.15–0.45 Nb
	S17700	17–7 PH	0.09	1.0	1.0	16.0–18.0	6.5–7.75			0.75–1.5 Al
Duplex	S31803	S32205 or 2205	≤ 0.03	2.0	1.0	21.0–23.0	4.5–6.5	2.5–3.5	0.08–0.2	
	S32101	2101 [(1)]	≤ 0.04	4.0		21.0 – 22.0	1.35 – 1.7	0.1 – 0.8	0.2 – 0.25	0.1 – 0.8 Cu
	S32304	2304	≤ 0.03	2.5		21.5–24.5	3.0–5.5	0.05–0.6	0.05–0.2	0.05–0.6 Cu
Super duplex	S32520	S32520	≤ 0.03	1.5		24.0 – 26.0	5.5 – 8.0	3.0 – 5.0	0.2 – 0.35	0.5 – 3.0 Cu
	S32750	S32750 or 2507 [(2)]	≤ 0.03			24.0–26.0	6.0–8.0	3.0–5.0	0.2–0.35	
	S32760	S32760	≤ 0.03	1.0		24.0 – 26.0	6.0 – 8.0	3.0 – 4.0	0.2 – 0.3	0.5 – 1.0 Cu 0.5 – 1.0 W
	S39274	S39274	≤ 0.03	1.0		24.0 – 26.0	6.0 – 8.0	2.5 – 3.5	0.24 – 0.32	0.2 – 0.8 Cu 1.5 – 2.5 W

[(1)] *LDX 2101 (JIS),* [(2)] *SAF 2507 (Sandvik).*

performing tests at different temperatures. Additionally, long-term potentiostatic experiments were conducted as a function of temperature in natural seawater to validate PD-GS-PD testing. Results showed that W improved crevice corrosion resistance, as evidenced by the higher initiation and repassivation crevice temperatures, which were 7.5–15 °C higher in the 2.1 wt% W SDSS than in the W-free case. They observed that crevice attack initiated at ferrite (α)/austenite (γ) boundaries. The ferrite was selectively corroded, and the austenite dissolution occurred at a later stage during crevice propagation, as shown in Fig. 11.

The addition of N to austenitic stainless steels promotes the passive film formation. N and Mo interact to form a protective film layer on the surface of the steel. The formation of Mo nitrides helps to retain the Mo ion in the passive film by acting as an inhibitor to the dissolution of Mo in the transpassive region. Whereas, the addition of elements such as S and Mn decreases the corrosion resistance of

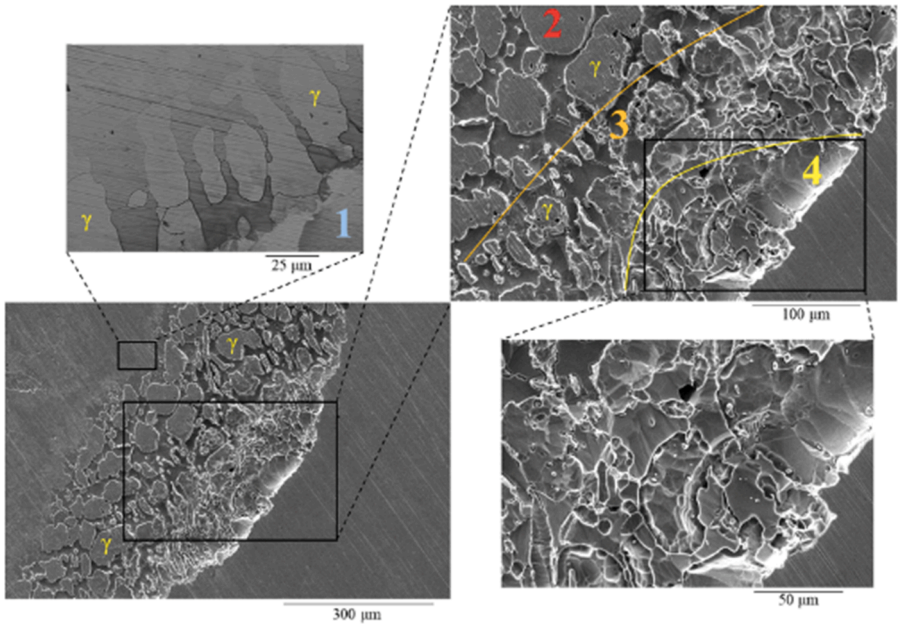

Fig. 11. SEM images of a crevice attack of UNS S32750 after corrosion in 3.5 % wt. NaCl, pH = 6, and 60 °C. The crevice propagation stages are indicated by numbers: (1) phase boundary attack, (2) selective dissolution of α phase, (3) partial dissolution of γ phase, and (4) γ phase is completely dissolved [45].

metals [64,69].

Metallurgical variables have various effects on the passive film stability such as heterogeneity at grain boundaries and/or disorder in the passive film by impurity atoms or inclusions. For example, sulfide inclusion (MnS) in the material microstructure acts as sites for pit nucleation [70,71].

Furthermore, numerous microstructural changes can occur in duplex and super duplex stainless steels during isothermal heat treatments. Most of these transformations are related to ferrite, since the diffusion rate in this phase is approximately 100 times faster than in austenite, which is mainly due to the lower lattice parameter of the CCC crystalline structure. In addition, ferrite is enriched in Cr and Mo, which are known to promote the precipitation of intermetallic phases. The solubility of these elements decreases in the ferrite as the temperature decreases, increasing the probability of precipitation of these compounds during the heat treatment. Many of these precipitates compromise the mechanical properties and the corrosion resistance [72]. Although there are several studies on the influence of major alloying elements on crevice resistance, the synergistic effects of various alloying elements on crevice corrosion of CRAs steels are not fully understood.

Austenitic stainless steels such as UNS S30403 (AISI 304L) and UNS S31603 (AISI 316L), lean duplex or duplex stainless steels (UNS S32101 – AISI 2101, S32304 – AISI 2304 or S32205 – AISI 2205) with PREN below 38 are usually not recommended for seawater handling systems. In aerated seawater, these grades require cathodic protection [61]. However, they might be used for some particular applications with deaerated seawater for offshore oil and gas applications. Stainless steels with PREN above 40 are called super stainless steel (UNS S31254 – AISI 254 SMO, S31266 – AISI S31266, S32520 – AISI S32520, and S32750 – AISI 2507). However, cases of pitting and crevice corrosion have been observed for super stainless steels in field service conditions. The operational corrosion risk on these highly alloyed stainless steels depends on the operating conditions (i.e. temperature, chlorination, oxygen content and flowing conditions), on the metallurgy (i.e. cast or wrought alloys) and on the geometrical configuration of the confined zones in contact with seawater. Larché et al. [61] studied crevice corrosion of many duplex stainless steels in natural and chlorinated seawater. Results from this investigation showed that the alloys can be ranked as regards crevice corrosion resistance as followed: UNS - S32101 (duplex) ~ S30403 (austenitic) < S31603 (austenitic) ~ S32304 (duplex) < S32205 (duplex) < S31254 (super austenitic) ~ S32520 (super duplex) ~ S32750 (super duplex) < S31266 (super austenitic).

5.3. *Environmental factors*

Comprehension and prediction of the corrosion behavior of CRAs in different environmental conditions are of great importance. The literature shows that by increasing chloride concentration, temperature, and acidity of the solution, localized corrosion resistance of CRAs generally decreases [10,73]. Among all the influencing environmental parameters, chloride concentration, temperature, pH, and oxygen play a key role in the determination of pitting and crevice corrosion performances of stainless steels and will be discussed in the following sections.

However, the comparison of literature results can be difficult due to the diversity of materials, experimental parameters and

methods used to evaluate crevice corrosion. The effects of the above environmental parameters on crevice corrosion have been discussed individually in the relevant literature. However, the use of Design of Experiments (DOE) techniques is little explored for designing experiments and analyzing experimental data. DOE is appropriated to determine the influence of individual parameters and interactive effects of various factors that can influence the crevice corrosion. Dastgerdi et al. [10] have used DOE and multi-variable analysis as a method to evaluate the effects of multiple environmental parameters (chloride, temperature, and pH) on the pitting and crevice corrosion of AISI 304L stainless steel. They observed that passivity breakdown potential is influenced by pH, temperature and chloride concentration, as expected. Among all these parameters, the temperature had the most significant effect, especially in the range 20 °C-40 °C.

A literature review on the main studies about the influence of the main environmental factors on crevice corrosion is presented in the following items.

5.3.1. Temperature

The influence of temperature on the crevice corrosion initiation process is complex because due to the presence of multiple other factors. During the corrosion process, increase in temperature accelerates the kinetics of metal dissolution and reduction reactions, causing the breakdown of the passive region. An increase in temperature also can causes an increase in the conductivity of electrolytes, leading to an increase in the rate of electrochemical reactions and anodic current. However, by increasing temperature, localized corrosion resistance of stainless steels can decrease in certain conditions because oxygen solubility is reduced. Thereby decreasing the external cathodic reaction rate results in lower corrosion rates. The role of temperature rise is mainly to control the rate of pitting initiation by stabilizing of pits and hindering their repassivation [10].

Critical crevice temperature is an important parameter for materials selection since it defines the maximum operation temperature below which a material us not susceptible to crevice corrosion. Fig. 12 illustrates the CCT and CPT for various CRAs in $FeCl_3$ solution. In the presence of crevices, the critical temperature is lower compared to pitting [57,72]. Consequently, a material qualified to be resistant to crevice corrosion at a certain temperature is also considered to be resistant to pitting. The relation of critical crevice potential and solution temperature was investigated by Han et al. [58] for SAF 2205 DSS (UNS S32205 or S31803 and AISI 2205). The polarization curves of creviced SAF 2205 DSS specimen obtained in 4 % NaCl solutions at different solution temperatures show that the increase in temperature significantly results in a decrease in breakdown potential. The relationship between the breakdown potential and solution temperature was used for the determination of CCT. The CCT was about 28 °C, which is in agreement with previous investigations of the authors [57], where they reported a CCT of 29–3 °C for the same steel through electrochemical potentiostatic measurement by using another set of crevices former.

The repassivation potentials from PD-PS-PD tests as a function of temperature in chloride solutions at different temperatures were obtained by Martínes et al. [74] for UNS S32750 (AISI 2507) super duplex, UNS S31254 (AISI 254 SMO) and UNS S32654 (AISI S32654) super austenitic stainless steels and are shown in Fig. 13. The crevice corrosion repassivation potential of S31254 and S32654 alloys decreased at higher temperature and chloride concentration, while S32750 presented a constant behavior with temperature increase. At 30 °C, S32654 alloy showed a significantly higher repassivation potential than S32750 and S31254, both in 10,000 and 100,000 ppm Cl^- solutions.

It is well known that CCT increases with PREN of steel. Jakobsen & Maahn [75] studied the crevice corrosion of UNS S31600 (AISI 316) austenitic stainless steel (PREN = 26) at different temperatures using a special electrochemical cell for crevice corrosion testing. They reported a CCT of 5 ± 1 °C for S31600, which is much lower than SAF 2205 (UNS S32205 or S31803 and AISI 2205) duplex stainless steel (28 °C) for example. Therefore, the PREN classification should be used with precaution since PREN does not consider other important parameters such as the metallurgical aspects, the nickel content, or the surface state.

Electrochemical and passivation behavior of UNS S32750 (AISI 2507) super duplex stainless steel in simulated desulfurized flue gas condensates in the chimney was investigated by Cui et al. [76]. Electrochemical Impedance Spectroscopy analysis shows a transition of the film structure from single layer to bilayer at temperatures above 40 °C, possibly attributed to the generation of a porous outer layer from dissolution and precipitation of the Fe oxyhydroxides. Passive film consisted of hydroxide and oxide of Fe and Cr on the surface, and Cr oxides close to the film/metal interface. The authors concluded that the influence of temperature on the passive film properties

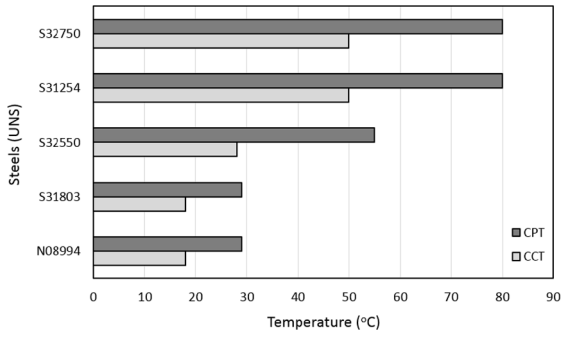

Fig. 12. Critical crevice corrosion temperature (CCT) and critical pitting corrosion temperature (CPT) in $FeCl_3$ solution for various CRAs (). adapted from [72]

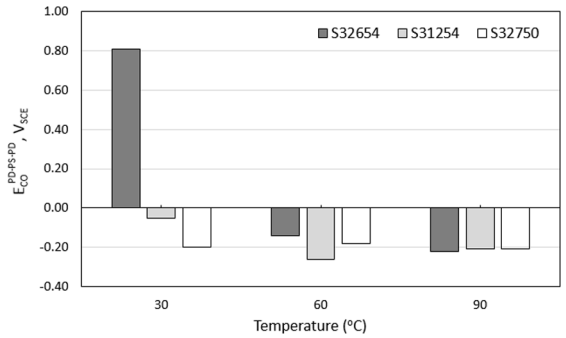

Fig. 13. Repassivation potential from PD-GS-PD tests as a function of temperature ().
adapted from [74]

is mainly controlled by the variation of film structure and doping concentrations.

Oberndorfer et al. [77] investigated the application limits of stainless steels in the petroleum industry. Austenitic stainless steel grades UNS S32100 (AISI 321), UNS S31635 (AISI 316Ti -API LC30-1812) and UNS S31254 (AISI 254 SMO), and the austenitic-ferritic UNS S31803 (AISI 2205) duplex stainless steel were tested in autoclave (10 bar) for pitting and stress corrosion cracking in NaCl solutions containing from 3 to 100,000 ppm Cl^- at temperatures from 40 to 200 °C. Type AISI 304 or AISI 321 austenitic steels are resistant to localized corrosion up to 40 °C, the temperature limits for 316Ti, 2205 duplex and 254 SMO are 55 °C, 90 °C and 125 °C, respectively.

5.3.2. Chloride concentration

The chloride ions aggressiveness is related to the small size, high diffusivity, and strong anionic nature of these ions. Numerous studies on the effect of chlorides ions on pitting behavior of stainless steels have shown a logarithmic relationship between passivity breakdown potential and chloride ion concentration [13,49,58,61,74,77].

Han et al. [57] studied the effect of chloride ion concentration on the crevice corrosion resistance of SAF 2205 (UNS S32205) duplex stainless steel. The results presented in Fig. 14 show that the CCT linearly decrease with the logarithm of chloride concentration.

Hornus et al. [49,78] studied the effect of both temperature and chloride concentration on the crevice corrosion resistance of austenitic stainless steels. The crevice corrosion repassivation potential was determined by the PD-GS-PD method. The repassivation potential of UNS S30400 (AISI 304) austenitic alloy decreased with increasing chloride concentration and temperature in the 0–60 °C range, but reached a constant value between 60 and 90 °C, independently of the chloride concentration. This minimum and constant repassivation potential value was the corrosion potential in the crevice-like solution (-0.430 ± 0.015 V_{SCE}) for UNS S30400 steel. The repassivation potential of UNS S31600 (AISI 316) steel showed a decrease with increasing chloride concentration and temperature within the whole temperature range. Crystalline attack prevailed in UNS S31600 and pitting corrosion prevailed in UNS S30400.

Pardo et al. [79] investigated pitting and crevice corrosion of two high-alloy stainless steels, 25 % Cr super duplex (25SD) and 24 % Cr super austenitic (24SA) in solutions with chloride concentrations of 200, 400, 600, and 6,000 ppm at pH values ranging from 2 to 6.5. Table 2 lists values of crevice potential, repassivation potential, and CCT. In all cases, the CCT was lower than CPT, indicating that

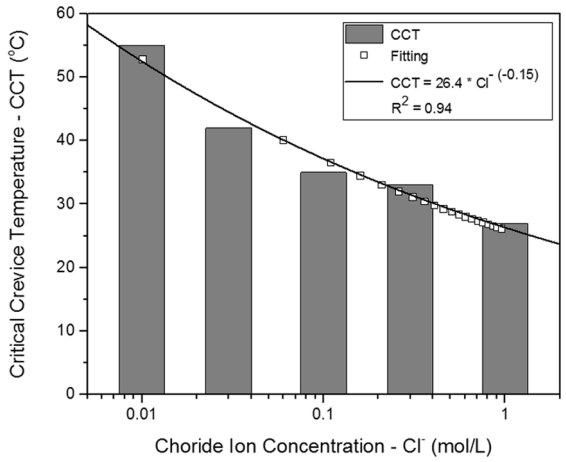

Fig. 14. Effect of chloride ion concentrations on the CCT for SAF 2205 (UNS S32205) duplex stainless steel ().
adapted from [58]

both stainless steels were more susceptible to crevice than pitting attack. For materials tested at pH 2 at various chloride concentration levels, 24 % Cr super austenitic presented a CCT superior to the value obtained for 25 % Cr super duplex steel. When materials operated at pH values of 3.5 and 6.5, a more resistant behavior of super austenitic stainless steel was observed at chloride concentrations lower than 600 ppm. On the other hand, the performance of super duplex stainless steel was superior to the one exhibited by super austenitic when the chloride concentration was higher than 600 ppm. This difference can be attributed to the change in concentration of the aggressive ion. At pH 6.5 and 6,000 ppm chloride, the CCT of both materials was lower than at room temperature.

The highest chlorine level which can be used in seawater depends on the stainless steel grade and temperature. NORSOK Standard M−001 rev. 4 (Norwegian Petroleum Industry Standard) suggests an upper temperature limit of 20 °C for super duplex and 6 %Mo alloys with tight crevices (such as screw couplings) with 1.5 mg/L chlorine. Other experiences with these alloys showed that the maximum temperature largely depends on chlorine concentration. However, the safe maximum temperature will also largely depend on the severity of the crevice geometry. It is well known that the open-circuit potential (OCP) of stainless steels shifts to the noble direction (ennoblement) when exposed to natural seawater, increasing the probability of localized corrosion initiation. This shift of OCP has been correlated with the development of a biofilm on the stainless steel surfaces [61].

5.3.3. pH

pH variations are responsible for a change in the chemistry of an aqueous medium, which can affect both electrochemical and corrosion properties of stainless steels. The decrease in pH, due to the hydrolysis of metal elements, and increase in chloride concentration due to the ions migration, lead to the formation of critical chemistry for the initiation of corrosion in crevice [58].

The passivity breakdown potential increases in alkaline conditions, while the passive film is weakened by acidic condition. In severe acidic condition, the passive film becomes thermodynamically unstable, according to the Pourbaix diagram. Some authors believe that in an acidic medium the reduction in pitting potential is due to the decrease in the passive film thickness. Whereas, other researchers consider the competition between chloride and OH^- ions, with the role of chloride becoming predominant at lower pH [75,79–81].

The effect of pH on the crevice corrosion behavior of SAF 2205 (UNS S31803 or AISI 2205) duplex stainless steel was determined to be quite significant [58]. The results of CCT measurements in 4 % NaCl at different pH ranging from 1.5 to 10 are presented in Fig. 15, which shows the CCT as a function of pH values. It can be seen that the CCT increased gradually with the increase in pH from 1.5 to 8.5, decreasing dramatically with the increase in pH from 8.5 to 10. The maximum CCT was observed at pH 8.5.

Pardo et al. [79] investigated pitting and crevice corrosion of two high-alloy stainless steels (superduplex and superaustenitic) in solutions with chloride concentrations of 200, 400, 600, and 6,000 ppm at pH values ranging from 2 to 6.5, as showed in Table 2 for crevice corrosion. Comparing the CPT and CCT of both materials, the CPT was greater than the CCT in all tested conditions of pH, temperature, and concentration of Cl^- (i.e., the materials studied were more susceptible to crevice than pitting corrosion). As an example, the comparison of the critical temperatures with the pH and maximum concentration of chloride tested is shown for the two materials in Fig. 16.

5.3.4. Dissolved oxygen

The amount of oxidant and/or its availability to the bold surface drives the anodic dissolution reaction in the crevice, which in turn increases the rate of crevice corrosion. Therefore, a decrease in crevice corrosion susceptibility can be attributed to the decrease in the cathodic kinetics such as the availability of oxygen at the bold surface. Sawford et al. [82] investigated the role of oxygen on stability of iron crevice corrosion in 0.5 M Na_2SO_4 containing 0.1 mM NaCl (pH 6). The results showed that when an oxidant was added to the electrolyte in the crevice, the current flow out of the crevice decreased. As a result, the gradient of the IR-voltage and the tendency for IR-induced crevice corrosion decreased. They concluded that adding a subsequent saturated O_2-electrolyte of the same pH to the solution in the crevice provided a cathodic reduction rate on the crevice wall that was sufficient to terminate the crevice corrosion process.

In other cases, oxygen can affect the composition of the corrosion products, the composition and properties of surface films, frequently oxide films, and reduce the corrosion rate [83]. The dissolved oxygen has also effects on other properties, for example, fatigue. Otsuka et al. [84] observed the effect of dissolved oxygen on fatigue crack initiation process and propagations processes of austenitic stainless steels (UNS 30,400 - AISI 304 and UNS 31,603 - AISI 316L) in 0.9 %wt. sodium chloride solution. Crack growth rate

Table 2
Results of cyclic polarization studies of crevice corrosion of 25% Cr super duplex (25 SD) and 24% Cr super austenitic (24 SA) stainless steels (adapted from [79]).

	Stainless Steels	200 ppm pH			400 ppm pH			600 ppm pH			6000 ppm pH		
		2	3.5	6.5	2	3.5	6.5	2	3.5	6.5	2	3.5	6.5
E_{crev}	25 SD	0.81	0.84	0.60	1.20	1.10	1.25	0.81	1.15	1.06	1.10	1.10	–
(V_{SCE})	24 SA	–	1.15	1.11	–	1.13	1.12	–	1.10	1.08	–	1.04	–
E_{rep}	25 SD	0.81	0.74	0.42	1.20	1.08	1.25	0.81	1.15	1.06	1.10	1.02	–
(V_{SCE})	24 SA	–	1.10	1.03	–	1.09	1.06	–	1.06	1.05	–	0.99	–
CCT	25 SD	90	75	70	85	65	60	80	60	55	65	25	< 25
(°C)	24 SA	–	90	85	–	75	75	–	35	35	–	25	< 25

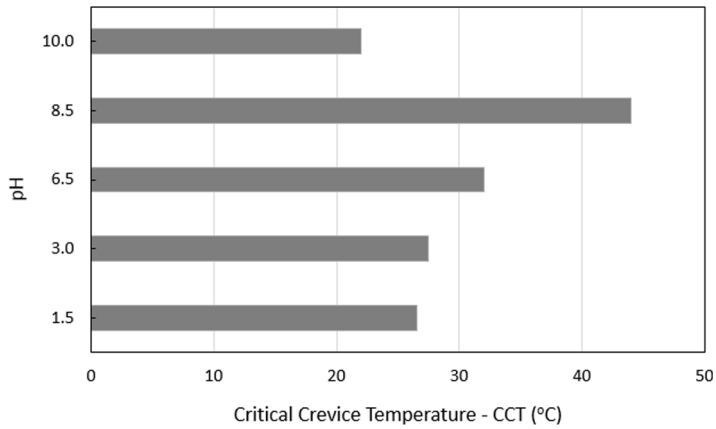

Fig. 15. Effect of pH on the CCT for SAF2205 duplex stainless steel in 4% NaCl ().
adapted from [58]

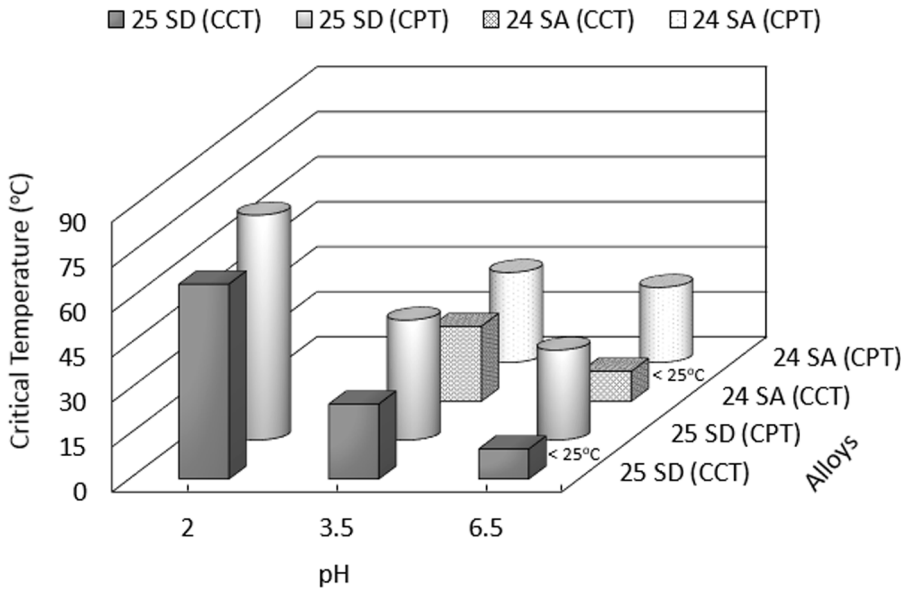

Fig. 16. CPT and CCT vs pH at 6,000 ppm of Cl^-. a) 25 % Cr super duplex steel (SD) and b) 24 % super austenitic steel (SA) ().
adapted from [79]

in lower dissolved oxygen environment became lower in both stainless steel cases that mean crack propagation is accelerated by dissolved oxygen.

In oil and gas field operations, produced water originating from multiple wells or sources can be mixed at water injection points. The composition of produced water, even from single sources, often varies with time. Gathering produced water from multiple sources accentuates this effect to the extent that disposal water exhibits a particularly wide range of compositions. Frequently, the gathered disposal water does not have a controlled oxygen content. Some oil companies, as Shell [9] apply the following definitions for oxygen control:

- Proper oxygen control: $<$ 10 ppb dissolved oxygen.
- Proper oxygen control not in place: $<$ 50 ppb dissolved oxygen.
- No oxygen control: $>$ 50 ppb (to saturation).

In offshore oil and gas industry, the injection of deaerated seawater to maintain the well pressure and sustain production is common). For some high-water producer fields, water is injected into the oil-bearing strata instead. Where there are only small quantities of produced water, it is necessary to mix the deaerated produced water with deaerated seawater. Because the produced water is characterized by a high temperature, and often by a high chloride content, there is concern about the corrosion of stainless steels used in mixed water injection systems [85].

The presence of oxygen, combined with a residual chloride content, significantly increases the risk of localized corrosion in many

CRAs in which corrosion performance is derived from the presence of a passive oxide film. Under certain combinations of temperature, chloride content and oxygen level, the passive oxide film breaks down, which can lead to localized corrosion with high penetration rates. However, the limits of acceptable oxygen are not yet well established and depending on the grade of CRAs employed, the tolerance level of the DO may vary [9,73].

Francis et al. [85] have tested samples of super duplex stainless steel (Z100) in seawater with extra sodium chloride to increase the chloride content to 100,000 mg/L with oxygen contents of 50, 200 and 410 ppb and 0.1 MPa CO_2 at high temperatures. The alloy has a nominal composition of Fe/25Cr/7Ni/3.5Mo/0.25 N/0.7Cu/0.7 W, with a PREN > 40. The samples were creviced wrought and cast Z100 and plain welded wrought Z100. The results after 30 days exposure are shown in Fig. 17. It can be seen that wrought material presented crevice and pitting corrosion resistance at welds under all the test conditions, while the cast alloy suffered some crevice corrosion.

Fletcher et al. [9] investigated the crevice corrosion oxygen and temperature limits of CRAs (25Cr super duplex stainless steel - UNS S39274 and Inconels) for water injection wells. The electrochemical crevice corrosion initiation measurements were performed using the stepwise methodology developed by Shell Technology Centre in combination with the controlled crevice assembly first proposed by Oldfield (1989[33] and subsequently defined by the European CREVCORR project. The crevice is formed on surface-ground plate specimens using polyvinylidene fluoride (PVDF) crevice formers loaded with constant torque (4 Nm) via the use of disc springs. The disc springs compensate for any relaxation of the PVDF with time, thus preventing widening of the crevice. A representation of the crevice assembly, including both a platinum electrode wire for electrical contact and a counter electrode, is shown in Fig. 18a. For the electrochemical measurements the potential is raised in 50 mV steps and held for a dwell time of 3 h per step. The applied potential at which corrosion occurs defines the crevice corrosion initiation potential. A safety margin of −50 mV is then applied to the measured initiation potential to give the crevice potentials E_{crev}, as illustrated in Fig. 18b. Fig. 19 shows E_{crev} values for 25Cr superduplex stainless steel for different test solutions and temperatures under deaerated conditions.

A schematic diagram of the influence of dissolved oxygen on E_{corr} in saline solutions is shown in Fig. 20. Variations in dissolved oxygen below 50 ppb have a large effect on E_{corr}, but above 50 ppb there is relatively little change in E_{corr} even at full saturation. Fig. 21 presents the results indicating operating window of 25Cr super duplex in 60,000 ppm and 150,000 ppm chloride.

Lu & Paul [73] performed pitting corrosion tests to determine the DO limits for 316L (UNS S31603) austenitic stainless steel and 25 %Cr (UNS S32750) super duplex stainless steel (SDSS) in saline solutions. The DO levels examined were 20, 50 and 100 ppb in a range of chloride ion concentrations (up to 152 g/L Cl^-) at temperatures of 50 and 60 °C. The experiments showed a clear indication of dissolved oxygen and temperature dependency of localized corrosion. The surface finish and chloride content also had an effect. 316L was susceptible to pitting corrosion in the two salt solutions (i.e., 9.6 and 61 g/L chloride ions) with 100 ppb DO at 50 and 60 °C. However, 25Cr SDSS was resistant to pitting corrosion in the two saline solutions (i.e., 101 and 152 g/L chloride ions) with a DO content up to 100 ppb at 50 and 60 °C. As expected, the best pitting resistance was obtained for the higher alloy 25Cr SDSS (Pitting Resistance Equivalent Number-PREN = 41), compared with 316L (PREN = 24.8). The corrosion potential increases with the increase of the DO content in the saline solution. Therefore, the corrosion potential could potentially exceed the pitting potential, leading to corrosion pit initiation and propagation. The increased DO had a more significant effect on pitting corrosion of 316L than on 25Cr SDSS.

Al Wahaibi et al. [86] investigated welded 316L, 22Cr and 25Cr duplex stainless steels in environments containing 20, 50 and 100 ppb of dissolved oxygen at temperatures of 50 and 60 °C with different salt concentrations (16, 100, 167 and 250 g/L NaCl). The test duration was 30 days. After testing, the specimens were inspected by optical microscopy, SEM and profilometry. Fig. 22 shows the results which agree with the results of Lu & Paul [73]. The welded 316L steel was resistant to crevice corrosion at 20 ppb DO for all NaCl concentration and at both temperatures (50 and 60 °C). The 22Cr SDSS was also resistant to crevice corrosion at 20 ppb DO for all NaCl concentration and at both temperatures (50 and 60 °C), but at 50 ppb DO presented localized corrosion for in 250 g/L NaCl at 60 °C. At higher DO content (100 ppb) localized corrosion was present in 167 g/L NaCl at 60 °C and in 250 g/L NaCl at 50 and 60 °C. The 25Cr duplex stainless steels did not present localized corrosion in all tested conditions.

Arjmand et al. [65] studied the electrochemical behavior of AISI 316L stainless steel (UNS S31600) exposed to high-pressure NaCl solutions (12 MPa and 18 MPa) as a function of temperature (30–350 °C), chloride concentration (10–1000 ppb) and DO (0–200 ppb). An experimental design strategy called central composite design was used to analyze the effective factors versus the electrochemical

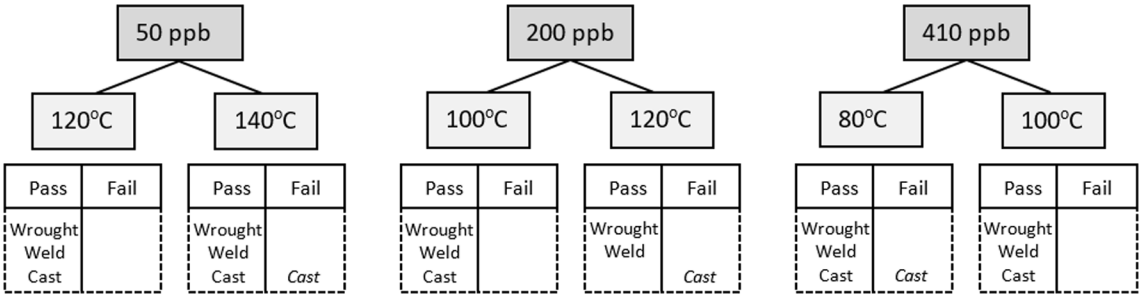

Fig. 17. Results of crevice and pitting corrosion tests of super duplex stainless steel (Z100) in a simulated mixed injection water (). adapted from [85]

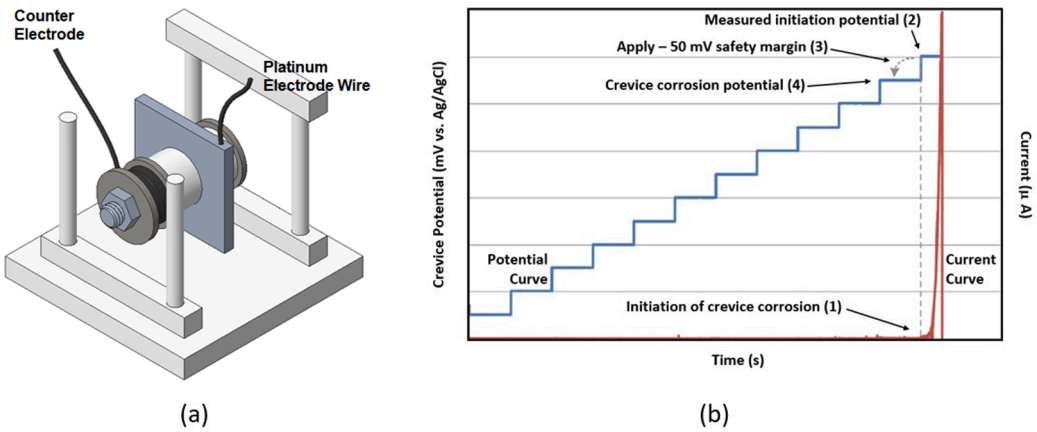

Fig. 18. Schematic representation of the: (a) crevice assembly prior to crevice testing and (b) current response to applied potential including determination of the crevice potential E_{crev} from the experimental data (stages 1–4) ().
adapted from [9]

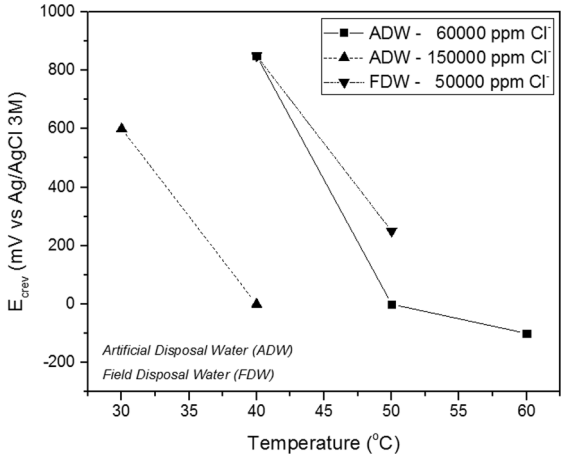

Fig. 19. E_{crev} values for each test solution and temperature under deaerated conditions ().
adapted from [9]

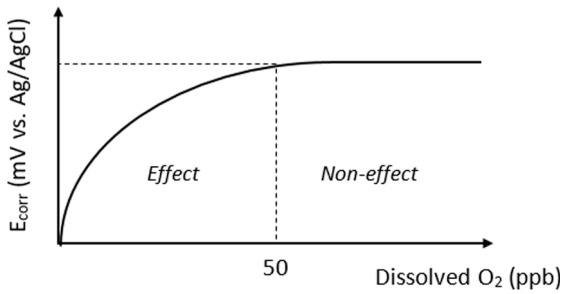

Fig. 20. Schematic diagram of the influence of dissolved oxygen on E_{corr} in saline solutions ().
adapted from [9]

responses. The optimum conditions in which the most positive transpassive potential (E_{trans}) and OCP values of AISI 316L stainless steel in high-temperature pressurized NaCl solutions can be achieved were found using the response surface experimental design method. The values were found as follow: T = 30 °C, $[Cl]^-$= 10 ppb and [DO] = 200 ppb. However, the most positive OCP values were observed when the values of the analyzed factors were: T = 140 °C, $[Cl]^-$= 10 ppb and [DO] = 200 ppb. Further analysis of the steel samples exposed to high temperature pressurized NaCl solutions under different experimental conditions was performed using EIS and

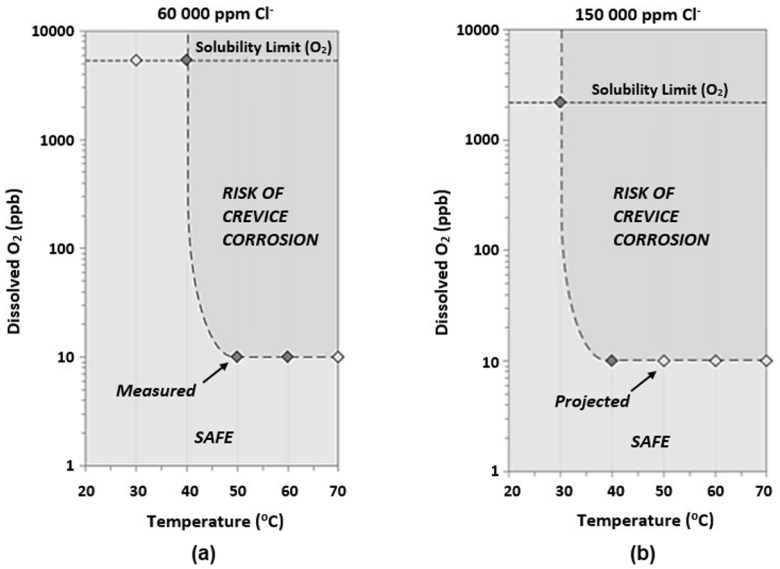

Fig. 21. Operating window of 25Cr super duplex in: (a) 60,000 ppm, and (b) 150,000 ppm Cl^- ADW - artificial disposed water (). adapted from [9]

SEM. They also observed that increasing the pressure from 12 MPa to 18 MPa moved the measured OCP and E_{trans} values towards more negative potentials and resulted in a less compact oxide film with averagely smaller particle size in comparison to the oxide film formed under lower pressures.

In marine environments, the role of oxygen in the kinetics of metal dissolution is of great importance. Indeed, metal dissolution is a critical element in the formation of passive films but also impacts biofilm formation on stainless steel surfaces. In addition, the oxygen depletion appears to be a prerequisite for the initiation and stabilization of crevice corrosion. Therefore, the investigation of the interactions between crevice corrosion of high-resistance alloys and biofilm formation in natural seawater shall be closely investigated, including the effect of oxygen [87].

Larché et al. [61] determined the evolution of stabilized open-circuit potential of the alloys (UNS S82551, UNS S31803 and UNS S39274) in natural seawater, as a function of dissolved oxygen content using a standard crevice assembly (CREVCORR) and the actual pipe-coupling premium connection (PCPC) crevice configuration. Additionally, they did full scale exposures tests of PCPC. Crevice corrosion occurred for S82551 and S31803 at DO of 100 ppb and above, while none of the tested specimens showed crevice corrosion at DO $<$ 50 ppb. Corrosion was initiated on S39274 for DO of 600 ppb. This confirms that the risk of crevice corrosion is significantly increased in conditions promoting potential ennoblement. The results from the corrosion tests of PCPC tubes in quiescent seawater were in good agreement with the CREVCORR-results, showing that 100 ppb is a borderline condition for crevice corrosion resistance of S82551 in natural seawater at 30 °C. Crevice corrosion of S39274 occurred only at 500 ppb and above.

Machuca et al. [12] also studied the effect of oxygen and biofilms on crevice corrosion of UNS S31803 and UNS N08825. They tested the samples with open circuit potential and anodic polarization measurements in natural seawater at 30 °C. The results of the investigation showed that the most severe crevice corrosion attack occurred in absence of oxygen and presence of a biofilm. They concluded that crevice corrosion is highly dependent on the oxygen content and that the most severe attack happened under fully anaerobic conditions compared to exposure in constantly aerated seawater. Meroufel et al. [88] studied crevice corrosion using hot rolled high grade stainless steels in two different natural seawaters with dissolved oxygen at saturation level (6 ppm). Biofilm growth occurred in both seawaters, and the biofilm ennoblement was observed with averaged stabilized potentials in the range of $+ 300 \pm 20$ mV_{SCE}. The results of the study confirmed the lower crevice corrosion resistance for duplex S32205 and the best crevice corrosion resistance for superaustenitic S31266.

Cui et al. [11] studied the passivation behavior and surface chemistry of AISI 2507 (UNS S32750) super duplex stainless steel in artificial seawater (ASW) focusing on the influence of dissolved oxygen and pH by using multiple characterization techniques. Removal of dissolved oxygen decreased the electric field strength and point defect diffusivity of the passive film. Passive current density in acidified ASW was higher than that in aerated ASW due to increased potential drop across film/solution interface, donor density and point defect diffusivity. The content of oxidized Cr, Fe(II) and hydroxides increase and film thickness reduces with acidification. In acidified ASW, passive film become denser from pre-passivation to passivation region and pores form accompanied with the increase of oxidized Fe after transpassivation.

The corrosion behavior of AISI 2205 (UNS S31803) duplex stainless steel was investigated in hot concentrated seawater with different dissolved oxygen concentrations by electrochemical measurement techniques and surface analysis methods by Zeng et al. [89]. The results were similar to the ones presented by Cui et al. [11]. Higher DO concentrations result in lower defect densities and thicker space charge layers in the passive films, which may effectively inhibit the intrusion of aggressive chloride ions. The increment

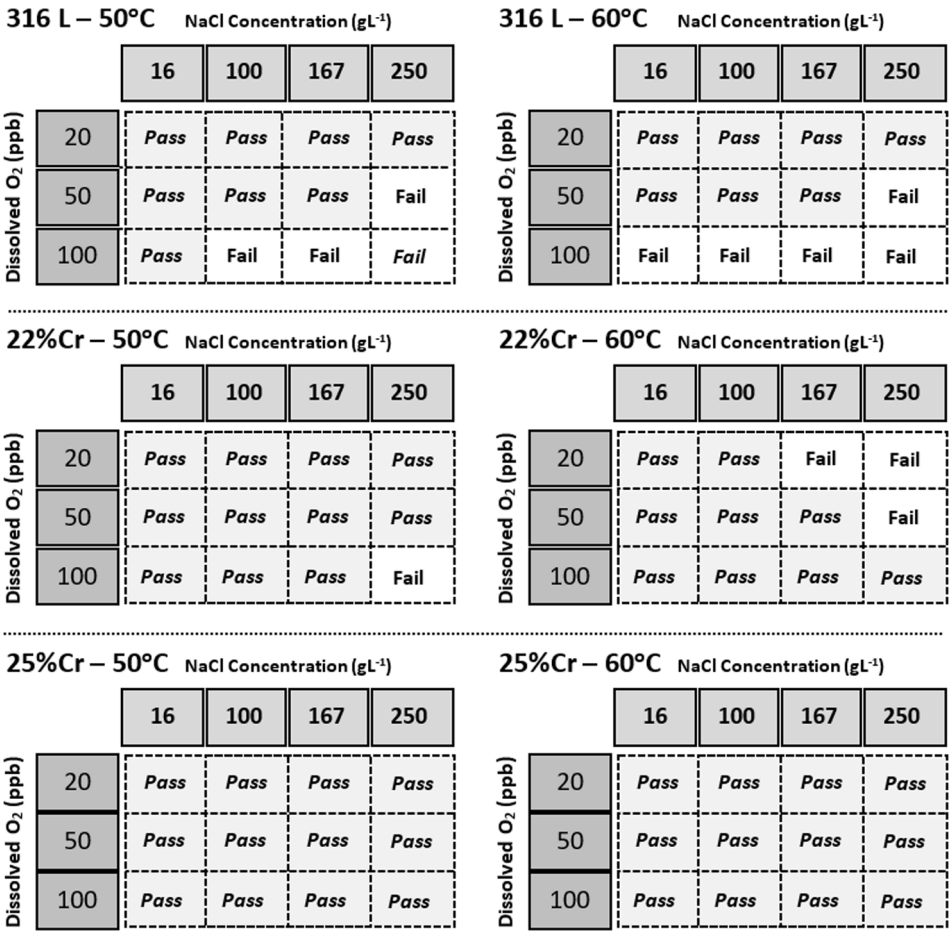

Fig. 22. Performance of various stainless steels concern to pits and crevice corrosion in different NaCl concentration solution and dissolved oxygen ().
adapted from [86]

in DO concentration clearly increases the pitting potential but decreases the repassivation potential. It may weaken both the occurrence and repassivation tendencies for stable pitting corrosion. Fig. 23 presents the perfect and imperfect passivity ranges for 2205 DSS in the hot concentrated seawater with different DO. The pitting potential value becomes higher with the increase of DO, indicating that DO decreases the pitting corrosion susceptibility of the specimens. The difference of repassivation potential and corrosion potential is defined as the perfect passivation region, which is the potential region that pitting corrosion will not initiate, and existing pits will not propagate. The difference pitting potential and repassivation potential is defined as imperfect passivity region, in which new pits cannot generate but the existed pits can propagate.

Mack & Carmimati [90] conducted tests in simulated seawater injection wells conditions for three levels of dissolved oxygen (30, 50, and 100 ppb) to assess the effect of upsets in control of the deaeration. The test temperature varied to simulate the temperature during constant injection (38 °C) and during shut-in (78 °C) during which oxygen replenishment does not occur. Four materials were studied: austenitic stainless steel UNS S31603, a 25Cr duplex stainless steel UNS S39274, and two precipitation hardened nickel base alloys, UNS N09925 and UNS N07718. Only UNS S31603 incurred significant localized corrosion.

Yang et al. [91] investigated corrosion behavior of AISI 2205 (UNS S31803) duplex stainless steel in the hot concentrated seawater under vacuum pressures by using electrochemical measurement techniques. The vacuum pressure results in the decrease of dissolved oxygen concentration and even boiling of solution. The AISI 2205 DSS passivates spontaneously under various vacuum pressures. The pressure reduction and the violent boiling of solution distinctly decrease the pitting potential but increase the repassivation potential. They may enhance both the occurrence and repassivation tendencies of stable pitting corrosion.

Recent works have promoted advances in crevice corrosion understanding. However, there are many remaining challenges associated with the comprehension and prediction of its phenomena and the effects of microstructure and environment to be able to estimate the time, location, and extent of crevice corrosion. Table 3 summarizes the main crevice corrosion test results found in literature for stainless steels involving electrochemical measurements. It can be seen a variety of steels, environmental parameters and methods have been used for the evaluation of crevice corrosion. As a consequence, to know exactly the effect of each environmental parameter as well as their combined effect on the crevice corrosion behavior of corrosion resistant steels is not obvious. Furthermore,

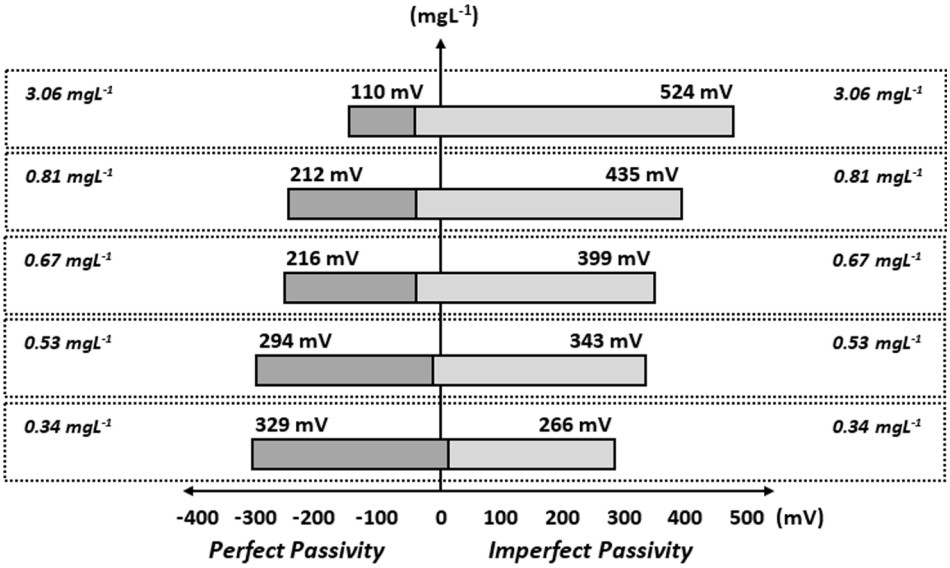

Fig. 23. Perfect and imperfect passivity ranges for 2205 DSS in the hot concentrated seawater with different DO (0.34 mg/L to 3.06 mg/L) (). adapted from [89]

despite the potential of electrochemical techniques very few electrochemical studies have been carried out varying the amount of dissolved oxygen, as shown in Table 3. The determination of the OCP, E_{crev} and E_{rep} under zero oxygen, varying pH, [Cl^-] and temperature, can be used to further establish the maximum allowable oxygen content. For example, the maximum oxygen content can be obtained when the OCP reaches E_{rep} (conservative limit) or E_{crev} (maximum limit). Besides, the laboratory experimental tests used to evaluate crevice corrosion are, in general, accelerated tests. The complexities of crevice corrosion in oil field require the development of experimental tests that simulate as close as possible the real operating conditions and the use of computational tools for appropriate prognostication and materials selection.

6. Conclusions

The aim of the present work was to review and discuss existing knowledge about crevice corrosion. The following general conclusions could be draw:

Crevice corrosion has received more attention in recent decades since it is frequently a limiting factor for the use of stainless steels in many industrial applications. Thus, a better understanding of the parameters that influence crevice corrosion and the development of testing methods that can reproduce and predict this type of failure is of fundamental importance to know long-term behavior of the materials in conditions close to real ones of oil & gas industry. In fact, crevice corrosion is a complex phenomenon and there are a multitude of conditions that can have a major bearing on what is generally considered a highly synergistic process.

Among all applied electrochemical techniques, CCP, LPP and PD-GS-PD are the most frequently used to evaluate the crevice performance of CRAs. The repassivation potential was preferred by some researchers over other criteria for ranking the materials, but a minimum crevice depth seems to be necessary to obtain reproducible values.

It is difficult to compare the literature results because of the diversity of materials, experimental design, environmental parameters and methods used for the evaluation of crevice corrosion. As a consequence, to summarize the effect of each environmental parameter (i.e., chloride content, temperature, pH, and dissolved oxygen) as well as their combined effect on the crevice corrosion behavior of CRAs is a challenging task.

Many studies show that by increasing chloride concentration, temperature, and acidity of the solution, localized corrosion resistance of CRAs generally decreases. Recently, Dastgerdi et al. (2019) [92] used DOE as a method to evaluate the effects of multiple environmental parameters on the pitting and crevice corrosion and found that the temperature had the most significant effect.

The oxygen dissolved in the medium also play an important role on the corrosive process, but literature is scarcer and the oxygen amount that could be safely administered when CRAs are used is still not well known. Although there is indication that oil and gas companies are in same cases conservative and that these limits could be altered for a some CRA grades under certain operation conditions (temperature and chloride concentration), as evidenced in some of recently published papers. However, it is important to note that this is only valid for immersed conditions tested in laboratory (usually accelerated tests) that can be not directly comparable to the offshore environment, which can only indicate a trend.

For better understanding the influence of environmental factors on crevice corrosion process more electrochemical studies are necessary and it is of fundamental importance the use of combined techniques to better comprehend the mechanisms involved in presence of dissolved oxygen. Furthermore, the definition of the test matrix to study the influence of combined parameters based on

Table 3
Summary of some electrochemical data about crevice corrosion test results found in literature for stainless steels.

Steel	Medium	T (°C)	pH	Technique	E_{corr} (mV)	E_{crev} (mV)	E_{rep} (mV)	RE	Oxygen	Observation	Source
304L	[Cl^-] = 1,000 ppm	10[j] 20 [k] 35 [l] 40[m] 50[n] 60[o]	4[4] 8[5] 6[6] 10[7]	CP	−0.034 [j,6] −0.036 [k,6] −0.081 [l,6] −0.060 [m,6] −0.074[n,6] −0.044 [°,6] 0.002 [k,4] −0.067 [k,5] −0.140 [k,6]	0.382[j,6] 0.218 [k,6] 0.050 [l,6] 0.039 [m,6] −0.022[n,6] 0.011 [°,6] 0.283 [k,4] 0.320 [k,5] 0.410 [k,6]	not informed	Ag/AgCl sat.	Aerated (6000–8000 ppb)		Dastgerdi et al., 2019
316	[NaCl] = 58,440 ppm	25	6	OCP	−400	−300	not informed	SCE	aerated	pH adjusted with HCl	Oldfield, 1978
316	[NaCl] = 58,440 ppm	−0,5	7[d] 4[e] 2[f]	LP	50[d,e,f]	900[d] 850[e] 750[f]	not informed	SCE	aerated	Acidified with HCl	Jackobsen & Maahn, 2001
316L	Natural Seawater with [NaCl] = 31,330 ppm	25	not informed	LP	−400	236	not informed	SCE	aerated	–	Nagajaran & Rajendran, 2009
316	Artificial Seawater with [NaCl] = 24,530,000 ppm	50	not informed	CP	−330	−15	−380	SCE	aerated	–	Cai et al., 2010
13 Cr	[NaCl] = 35,000 ppm	–	not informed	LP	−80[a,1] −100[b,1] −120[c,1] −130[a,2] −150[b,2] −180[c,2] −150[a,3] −170[b,3] −220[c,3]	280[a,1] 140[b,1] 60[c,1] 220[a,2] 100[b,2] 80[c,2] 160[a,3] 70[b,3] −20[c,3]	not informed	Ag/AgCl 1 mol/L	aerated	crevice under various applied stresses at different immersion times: [a:]24 h [b:]12 h [c:]2h [1:]0 MPa [2:]100 MPa [3:]300 MPa	Li et al., 2009
13 Cr	[NaCl] = 35,000 ppm	–	6.7	LP	−300	−80	not informed	SCE	aerated	–	Hu et al., 2011
25Cr	[NaCl] = 35,000 ppm	60	6.5	CP	−550	600	−100	Ag/AgCl sat.	< 10 ppb	–	Torres et al., 2021
25Cr	*Artificial disposal water: [Cl^-] = 60,000 ppm [#]Artificial disposal water: [Cl^-] = 150,000 ppm [§]Field disposal water: [Cl^-] = 50,000 ppm	30[p] 40[m] 50[n] 60[o]	not informed	Polarized in a stepwise	not informed	850[*,m] 0[*,n] −100[*,o] 600[#,p] 0[#,m] 850[§,m] 250[§,n]	not informed	Ag/AgCl 3 M	deaerated		Fletcher et al., 2014

DOE is strongly recommended in order to allow a post multi variable and statistical analysis of results.

Declaration of Competing Interest

The authors declare that they have no known competing financial interests or personal relationships that could have appeared to influence the work reported in this paper.

Data availability

Data will be made available on request.

Acknowledgements

We gratefully acknowledge support from Equinor and ANP (Brazil's National Oil, Natural Gas and Biofuels Agency) through the R&D levy regulation.

DATA AVAILABILITY STATEMENT: Research data are not shared.

References

[1] L.T. Popoola, A.S. Grema, G. Kayode Latinwo, B. Gutti, A. Saheed Balogun, Corrosion problems during oil and gas production and its mitigation, International Journal of Industrial, Chemistry 4–35 (2013) 1–15, https://doi.org/10.1186/2228-5547-4-35.
[2] R.G. Kelly, J.S. Lee, Localized corrosion: Crevice corrosion, in: Encyclopedia of Interfacial Chemistry: Surface Science and Electrochemistry, Elsevier, 2018: pp. 291–301. https://doi.org/10.1016/B978-0-12-409547-2.13420-1.
[3] N. Sridhar, R. Thodla, F. Gui, L. Cao, A. Anderko, Corrosion-resistant alloy testing and selection for oil and gas production, Corros. Eng. Sci. Technol. 53 (2018) 75–89, https://doi.org/10.1080/1478422X.2017.1384609.
[4] R. Johnsen, Corrosion challenges for the oil and gas industry in the State of Qatar, in: Proceedings of the TMS Middle East - Mediterranean Materials Congress on Energy and Infrastructure Systems, MEMA 2015, John Wiley and Sons Inc., 2015: pp. 3–12. https://doi.org/10.1002/9781119090427.ch1.
[5] A.H. Alamri, Localized corrosion and mitigation approach of steel materials used in oil and gas pipelines- An overview, Eng. Fail. Anal. 116 (104735) (2020) 1–17, https://doi.org/10.1016/j.engfailanal.2020.104735.
[6] L.I. Farfan-Cabrera, G.A. Rodríguez-Bravo, J.G. Godínez-Salcedo, C.D. Resendiz-Calderon, J.S. Salgado-Sviercovich, M. Moreno-Ríos, A crevice corrosion assessment method for joints of mechanical components sealed with composite structure gaskets – The case of the engine cylinder head/mono-block joint, Eng. Fail. Anal. 119 (104981) (2021) 1–13, https://doi.org/10.1016/j.engfailanal.2020.104981.
[7] A.J. Betts, L.H. Boulton, Crevice corrosion: review of mechanisms, modelling, and mitigation, Br. Corros. J. 28 (4) (1993) 279–296, https://doi.org/10.1179/000705993799156299.
[8] A.P. Kölblinger, S.S.M. Tavares, C.A. della Rovere, A.R. Pimenta, Failure analysis of a flange of superduplex stainless steel by preferential corrosion of ferrite phase, Engineering Failure Analysis. 134 (2022) 106098, 1-12. https://doi.org/10.1016/j.engfailanal.2022.106098.
[9] S. Fletcher, M. Wilms, J. Smit, W. Grimes, Assessment of the Crevice Corrosion Oxygen and Temperature Limits of Corrosion-Resistant Alloys for Water Injection Wells, *in:* Paper presented at the Eurocorr 2014, European Corrosion Congress, 8-12, September 2014.
[10] A.A. Dastgerdi, A. Brenna, M. Ormellese, M.P. Pedeferri, F. Bolzoni, Experimental design to study the influence of temperature, pH, and chloride concentration on the pitting and crevice corrosion of UNS S30403 stainless steel, Corros. Sci. 159 (108160) (2019) 1–9, https://doi.org/10.1016/j.corsci.2019.108160.
[11] Z. Cui, S. Chen, Y. Dou, S. Han, L. Wang, C. Man, X. Wang, S. Chen, Y.F. Cheng, X. Li, Passivation behavior and surface chemistry of 2507 super duplex stainless steel in artificial seawater: Influence of dissolved oxygen and pH, Corros. Sci. 150 (2019) 218–234, https://doi.org/10.1016/j.corsci.2019.02.002.
[12] L.L. Machuca, S.I. Bailey, R. Gubner, E.L.J. Watkin, M.P. Ginige, A.H. Kaksonen, K. Heidersbach, Effect of oxygen and biofilms on crevice corrosion of UNS S31803 and UNS N08825 in natural seawater, Corros. Sci. 67 (2013) 242–255, https://doi.org/10.1016/j.corsci.2012.10.023.
[13] N.N. Khobragade, A. v. Bansod, A.P. Patil, Effect of dissolved oxygen on the corrosion behavior of 304 SS in 0.1 N nitric acid containing chloride, Materials Research Express. 5 (2018) 046526, 1-14. https://doi.org/10.1088/2053-1591/aab8de.
[14] Y.T. Al-Janabi, An Overview of Corrosion in Oil and Gas Industry – upstream, midstream, and downstream sectors, in: Corrosion Inhibitors in the Oil and Gas Industry, Wiley-VCH (2020): pp. 1–39. https://doi.org/10.1002/9783527822140.ch1.
[15] K. Nalli, Appendix VI: Corrosion and Its Mitigation in the Oil and Gas Industries, Process Plant Equipment. John Wiley and Sons Inc. (2012) 673–679. https://doi.org/10.1002/9781118162569.app6.
[16] Q. Hu, G. Zhang, Y. Qiu, X. Guo, The crevice corrosion behaviour of stainless steel in sodium chloride solution, Corros. Sci. 53 (2011) 4065–4072, https://doi.org/10.1016/j.corsci.2011.08.012.
[17] Y.Z. Li, X. Wang, G.A. Zhang, Corrosion behaviour of 13Cr stainless steel under stress and crevice in 3.5 wt.% NaCl solution, Corrosion Science 163 (2020) 108290 1-13. https://doi.org/10.1016/j.corsci.2019.108290.
[18] S.F. Wika, Pitting and Crevice Corrosion of Stainless Steel under Offshore Conditions. Master Thesis. Department of Materials Science and Engineering, Norwegian University of Science and Technology, Trondheim (2012). https://ntnuopen.ntnu.no 〉 566900_Fulltext01.
[19] B. Cai, Y. Liu, X. Tian, F. Wang, H. Li, R. Ji, An experimental study of crevice corrosion behaviour of 316L stainless steel in artificial seawater, Corros. Sci. 52 (2010) 3235–3242, https://doi.org/10.1016/j.corsci.2010.05.040.
[20] B. de Force, H. Pickering, A clearer view of how crevice corrosion occurs, JOM 47 (1995) 22–27, https://doi.org/10.1007/BF03221250.
[21] N. Rashidi, S. Alavi-Soltani, R. Asmatulu, Crevice Corrosion Theory, Mechanisms and Prevention Methods, Proceedings of the 3rd Annual GRASP Symposium, Wichita State University, 27 April 2007. https://soar.wichita.edu/bitstream/handle/10057/917/grasp%20216.pdf.
[22] G.F. Kennell, R.W. Evitts, K.L. Heppner, A critical crevice solution and IR drop crevice corrosion model, Corros. Sci. 50 (2008) 1716–1725, https://doi.org/10.1016/j.corsci.2008.02.020.
[23] R. Johnsen, Corrosion Challenges for the Oil and Gas Industry in the State of Qatar, in: Proceedings of the TMS Middle East - Mediterranean Materials Congress on Energy and Infrastructure Systems (MEMA 2015). Karaman, I., Arróyave, R., Masad, E. (eds), Springer, Cham. https://doi.org/10.1007/978-3-319-48766-3_1.
[24] T.E. Perez, Corrosion in the oil and gas industry: An increasing challenge for materials, JOM 65 (2013) 1033–1042, https://doi.org/10.1007/s11837-013-0675-3.
[25] J. de Assis Severiano, A.S. Silva, E.M. Sussushi, M.V. da Silva Sant'Anna, M.A. da Cunha, C.P. Bergmann, S. Griza, Corrosion damages of flow regulation valves for water injection in oil fields, Engineering Failure Analysis 96 (2019) 362–373. https://doi.org/10.1016/j.engfailanal.2018.11.002.
[26] H. Cheshideh, F. Nasirpouri, B. Mardangahi, A. Jabbarpour, Failure analysis and preventive recommendations against corrosion of steel tubes of gas risers in natural gas urban distribution lines, Eng. Fail. Anal. 122 (105240) (2021) 1–12, https://doi.org/10.1016/j.engfailanal.2021.105240.
[27] L. Chen, B. Dong, W. Liu, F. Wu, H. Li, T. Zhang, Failure analysis of corrosion products formed during CO2 pre-corrosion of X70 and 3Cr steels: Effect of oxygen contamination, Eng. Fail. Anal. 140 (106529) (2022) 1–16, https://doi.org/10.1016/j.engfailanal.2022.106529.

[28] H. Panahi, A. Eslami, M.A. Golozar, A. Ashrafi Laleh, An investigation on corrosion failure of a shell-and-tube heat exchanger in a natural gas treating plant, Engineering Failure Analysis 118 (2020) 104918 1-10. https://doi.org/10.1016/j.engfailanal.2020.104918.
[29] X. Wang, L. Fan, K. Ding, L. Xu, W. Guo, J. Hou, T. Duan, Pitting corrosion of 2Cr13 stainless steel in deep-sea environment, J. Mater. Sci. Technol. 64 (2021) 187–194, https://doi.org/10.1016/j.jmst.2020.04.036.
[30] J. Osta, Super-duplex steels that resist corrosion in demanding topside oil and gas installations, Technical Article No. S-TU216-TA. 9/2013, Sandvik Materials Technology, (2013) 1-7.
[31] M.V. Biezma, M.A. Andrés, D. Agudo, E. Briz, Most fatal oil & gas pipeline accidents through history: A lessons learned approach, Eng. Fail. Anal. 110 (104446) (2020) 1–14, https://doi.org/10.1016/j.engfailanal.2020.104446.
[32] D. Brondel, R. Edwards, A. Hayman, Hill, Donald, S. Mehta, T. Semerad, Corrosion in the oil industry, in: Oilfield Review, 6-2 (1994) 4–18.
[33] J.W. Oldfield, W.H. Sutton, Crevice Corrosion of Stainless Steels II, Experimental studies, British Corrosion Journal. 13–3 (1978) 104–111, https://doi.org/10.1179/000705978798276258.
[34] Y.Z. Yang, Y.M. Jiang, J. Li, In situ investigation of crevice corrosion on UNS S32101 duplex stainless steel in sodium chloride solution, Corros. Sci. 76 (2013) 163–169, https://doi.org/10.1016/j.corsci.2013.06.039.
[35] H.Y. Chang, K.T. Kim, N.I. Kim, Y.S. Kim, Relationship between the Applied Torque and CCT to obtain the Same Corrosion Resistance for the Plate and Cylindrical Shape Stainless Steels, Corrosion Science and Technology. 15–2 (2016) 58–68, https://doi.org/10.14773/cst.2016.15.2.58.
[36] D. Chen, E.H. Han, X. Wu, Effects of crevice geometry on corrosion behavior of 304 stainless steel during crevice corrosion in high temperature pure water, Corros. Sci. 111 (2016) 518–530, https://doi.org/10.1016/j.corsci.2016.04.049.
[37] R.P. Frankenthal, H.W. Pickering, On the Mechanism of Localized Corrosion of Iron and Stainless Steel, J Electrochemical Society 119 (1972) 1304, https://doi.org/10.1149/1.2403983.
[38] J.W. Oldfield, Test techniques for pitting and crevice corrosion resistance of stainless steels and nickel-base alloys in chloride-containing environments, Int. Mater. Rev. 32–1 (1987) 153–172, https://doi.org/10.1179/095066087790150313.
[39] J. Schully, Chapter 19-Crevice Corrosion, in: Corrosion Tests and Standards: Application and Interpretation-Second Edition, ed. R. Baboian. West Conshohocken, PA: ASTM International, 2005, 221–232, https://doi.org/10.1520/MNL11025M.
[40] T. Mathiesen, A. Andersen, Paper No. 4272, Challenges in pre-qualification corrosion testing of CRAs based on ASTM G48, in: Paper presented at the Corrosion 2014, San Antonio, Texas, USA, March 2014.
[41] ASTM G48-11(2020), Standard Test Methods for Pitting and Crevice Corrosion Resistance of Stainless Steels and Related Alloys by Use of Ferric Chloride Solution, West Conshohocken, PA: ASTM International, 2020.
[42] ASTM G78-20, Standard Guide for Crevice Corrosion Testing of Iron-Base and Nickel-Base Stainless Alloys in Seawater and Other Chloride-Containing Aqueous Environments, West Conshohocken, PA: ASTM International, 2020.
[43] ISO, Corrosion of metals and alloys — Crevice corrosion formers with disc springs for flat specimens or tubes made from stainless steel, 18070:2015.
[44] ASTM G71-81(2019), Standard Guide for Conducting and Evaluating Galvanic Corrosion Tests in Electrolytes, West Conshohocken, PA: ASTM International, 2019.
[45] C. Torres, R. Johnsen, M. Iannuzzi, Crevice corrosion of solution annealed 25Cr duplex stainless steels: Effect of W on critical temperatures, Corros. Sci. 178 (109053) (2021) 1–14, https://doi.org/10.1016/j.corsci.2020.109053.
[46] S. Esmailzadeh, M. Aliofkhazraei, H. Sarlak, Interpretation of Cyclic Potentiodynamic Polarization Test Results for Study of Corrosion Behavior of Metals: A Review, Prot. Met. Phys. Chem 54 (2018) 976–989, https://doi.org/10.1134/S207020511805026X.
[47] ASTM G61-86(2018), Standard Test Method for Conducting Cyclic Potentiodynamic Polarization Measurements for Localized Corrosion Susceptibility of Iron-, Nickel-, or Cobalt-Based Alloys, West Conshohocken, PA: ASTM International, 2018.
[48] ISO, Corrosion of metals and alloys — Method of measuring the pitting potential for stainless steels by potentiodynamic control in sodium chloride solution, 15158:2014.
[49] E.C. Hornus, M.A. Rodríguez, R.M. Carranza, R.B. Rebak, Comparative study of the crevice corrosion resistance of UNS S30400 and UNS S31600 stainless steels in the context of Galvele's model, Corrosion 73–1 (2017) 41–52, https://doi.org/10.5006/2179.
[50] S. Tsujikawa, Y. Hisamatsu, On the Repassivation Potential for Crevice Corrosion, Corros. Eng. 29–1 (1980) 37–40, https://doi.org/10.3323/jcorr1974.29.1_37.
[51] ASTM G192-08 *2020, Standard Test Method for Determining the Crevice Repassivation Potential of Corrosion-Resistant Alloys Using a Potentiodynamic-Galvanostatic-Potentiostatic Technique, West Conshohocken, PA: ASTM International, 2020.
[52] N. Sridhar, G.A. Cragnolino, Applicability of repassivation potential for long-term prediction of localized corrosion of alloy 825 and type 316L stainless steel, Corrosion 49 (1993) 885–894, https://doi.org/10.5006/1.3316014.
[53] A.K. Mishra, G.S. Frankel, Paper No. 10237, Crevice Corrosion Repassivation of Alloy 22 in Aggressive Environments, in: Paper presented at the Corrosion 2010, San Antonio, Texas, March 2010.
[54] M. Rincón Ortíz, M.A. Rodríguez, R.M. Carranza, R.B. Rebak, Determination of the crevice corrosion stabilization and repassivation potentials of a corrosion-resistant alloy, Corrosion 66 (2010) 1050021–10500212, https://doi.org/10.5006/1.3500830.
[55] C.M. Giordano, M. Rincón Ortíz, M.A. Rodríguez, R.M. Carranza, R.B. Rebak, Crevice corrosion testing methods for measuring repassivation potential of alloy 22, Corrosion Engineering Science and Technology. 46-2 (2011) 129–133. https://doi.org/10.1179/1743278210Y.0000000014.
[56] X. Wu, Y. Liu, Y. Sun, N. Dai, J. Li, Y. Jiang, A discussion on evaluation criteria for crevice corrosion of various stainless steels, J. Mater. Sci. Technol. (2020) 22–25, https://doi.org/10.1016/j.jmst.2020.04.017.
[57] D. Han, Y. Jiang, B. Deng, L. Zhang, J. Gao, H. Tan, J. Li, Detecting critical crevice temperature for duplex stainless steels in chloride solutions, Corrosion 67 (2011) 0250041–0250047, https://doi.org/10.5006/1.3552290.
[58] D. Han, Y.M. Jiang, C. Shi, B. Deng, J. Li, Effect of temperature, chloride ion and pH on the crevice corrosion behavior of SAF 2205 duplex stainless steel in chloride solutions, J. Mater. Sci. Technol. 47 (2012) 1018–1025, https://doi.org/10.1007/s10853-011-5889-6.
[59] ATSM G150-18, Standard Test Method for Electrochemical Critical Pitting Temperature Testing of Stainless Steels and Related Alloys, West Conshohocken, PA: ASTM International, 2018.
[60] S. Nagarajan, N. Rajendran, Crevice corrosion behaviour of superaustenitic stainless steels: Dynamic electrochemical impedance spectroscopy and atomic force microscopy studies, Corros. Sci. 51 (2009) 217–224, https://doi.org/10.1016/j.corsci.2008.11.008.
[61] N. Larché, D. Thierry, V. Debout, J. Blanc, T. Cassagne, J. Peultier, E. Johansson, C. Taravel-Condat, Crevice corrosion of duplex stainless steels in natural and chlorinated seawater, Revue de Metallurgie. Cahiers D'Informations, Techniques 108–7 (2011) 451–463, https://doi.org/10.1051/metal/2011080.
[62] S.H. Kim, J.H. Lee, J.G. Kim, W.C. Kim, Effect of the Crevice Former on the Corrosion Behavior of 316L Stainless Steel in Chloride-Containing Synthetic Tap Water, Met. Mater. Int. 24–3 (2018) 516–524, https://doi.org/10.1007/s12540-018-0062-2.
[63] ASM Handbook –Properties and Selection: Irons, Steels, and High-Performance Alloys, Volume 1. ASM International, 1990. https://doi.org/10.31399/asm.hb.v01.9781627081610.
[64] A. Muwila, The Effect of Manganese, Nitrogen and Molybdenum on the Corrosion Resistance of a Low Nickel (<2 wt%) Austenitic Stainless Steel. Master Thesis. Faculty of Engineering, The School of Process and Metallurgical Engineering, University of the Witwatersrand, Johannesburg, 2006.
[65] F. Arjmand, L. Zhang, J. Wang, Effect of temperature, chloride and dissolved oxygen concentration on the open circuit and transpassive potential values of 316L stainless steel at high-temperature pressurized water, Nucl. Eng. Des. 322 (2017) 215–226, https://doi.org/10.1016/j.nucengdes.2017.06.048.
[66] N. Ebrahimi, P. Jakupi, J.J. Noël, D.W. Shoesmith, The role of alloying elements on the crevice corrosion behavior of Ni-Cr-Mo alloys, Corrosion 71–12 (2015) 1441–1451, https://doi.org/10.5006/1848.
[67] J.H. Potgieter, P.A. Olubambi, L. Cornish, C.N. Machio, E.S.M. Sherif, Influence of nickel additions on the corrosion behaviour of low nitrogen 22% Cr series duplex stainless steels, Corros. Sci. 50 (2008) 2572–2579, https://doi.org/10.1016/j.corsci.2008.05.023.
[68] E.B. Haugan, Effect of Tungsten on the Pitting and Crevice Corrosion Resistance of Type 25Cr Super Duplex Stainless Steels, Corrosion 73–1 (2017) 53–67, https://doi.org/10.5006/2185.

[69] H. Bing Li, Z. Hua Jiang, Y. Yang, Y. Cao, Z. Rui Zhang, Pitting corrosion and crevice corrosion behaviors of high nitrogen austenitic stainless steels, Int. J. Miner. Metall. Mater. 16 (2009) 517–524, https://doi.org/10.1016/S1674-4799(09)60090-X.
[70] S.E. Lott, R.C. Alkire, The Role of Inclusions on Initiation of Crevice Corrosion of Stainless Steel: I, Experimental Studies, Journal Electrochemical Society 136–4 (1989) 973–979, https://doi.org/10.1149/1.2096896.
[71] E.G. Webb, T. Suter, R.C. Alkire, Microelectrochemical Measurements of the Dissolution of Single MnS Inclusions, and the Prediction of the Critical Conditions for Pit Initiation on Stainless Steel, Journal Electrochemical Society. 148 (2001) B186, https://doi.org/10.1149/1.1360205.
[72] J.M. Pardal, S.S.M. Tavares, E.A. Ponzio, V.M. Schmitt, A review of corrosion resistance in duplex and superduplex stainless steels, Revista Virtual de Química. 5 (2013) 658–677, https://doi.org/10.5935/1984-6835.20130047.
[73] Q. Lu, S. Paul, Paper No. 9062, Determining the dissolved oxygen (DO) concentration limit in saline solutions for safe operation of CRAs. Paper presented at the Corrosion 2017, New Orleans, Louisiana, USA, March 2017.
[74] P.A. Martínez, M.A. Rodríguez, E.C. Hornus, R.M. Carranza, R.B. Rebak, Paper No. 5740, Crevice corrosion resistance of super-austenitic and super-duplex stainless steels in chloride solutions, *in:* Paper presented at the Corrosion 2015, Dallas, Texas, March 2015.
[75] P.T. Jakobsen, E. Maahn, Temperature and potential dependence of crevice corrosion of AISI 316 stainless steel, Corros. Sci. 43 (2001) 1693–1709, https://doi.org/10.1016/S0010-938X(00)00167-0.
[76] Z. Cui, L. Wang, H. Ni, W. Hao, C. Man, S. Chen, X. Wang, Z. Liu, X. Li, Influence of temperature on the electrochemical and passivation behavior of 2507 super duplex stainless steel in simulated desulfurized flue gas condensates, Corros. Sci. 118 (2017) 31–48, https://doi.org/10.1016/j.corsci.2017.01.016.
[77] M. Oberndorfer, K. Thayer, M. Kästenbauer, Application limits of stainless steels in the petroleum industry, Mater. Corros. 55–3 (2004) 174–180, https://doi.org/10.1002/maco.200303781.
[78] E. Hornus, R. Carranza, M. Rodrigues, R. Rebak, Paper No. 7170, Effect of Temperature and Chloride Concentration on the Crevice Corrosion Resistance of Austenitic Stainless Steels, in: Paper presented at the Corrosion 2016, Vancouver, British Columbia, Canada, March 2016.
[79] A. Pardo, E. Otero, M.C. Merino, M.D. López, M.V. Utrilla, F. Moreno, Influence of pH and Chloride Concentration on the Pitting and Crevice Corrosion Behavior of High-Alloy Stainless Steels, Corrosion 56 (2000).
[80] B.E. Wilde, E. Williams, The use of current/voltage curves for the study of localized corrosion and passivity breakdown on stainless steels in chloride media, Electrochim. Acta 16 (1971) 1971–1985, https://doi.org/10.1016/0013-4686(71)85151-4.
[81] M. Mobin, H. Shabnam, Corrosion behavior of mild steel and SS 304L in presence of dissolved nickel under aerated and deaerated conditions, Mater. Res. 14–4 (2011) 524–531, https://doi.org/10.1590/S1516-14392011005000076.
[82] M.K. Sawford, B.G. Ateya, A.M. Abdullah, H.W. Pickering, The Role of Oxygen on the Stability of Crevice Corrosion, Journal Electrochemical Society 149–6 (2002) B198, https://doi.org/10.1149/1.1470655.
[83] K.V. Rybalka, L.A. Beketaeva, A.D. Davydov, Effect of Dissolved Oxygen on the Corrosion Rate of Stainless Steel in a Sodium Chloride Solution, Russ. J. Electrochem. 54 (2018) 1284–1287, https://doi.org/10.1134/S1023193518130384.
[84] Y. Otsuka, S. Nagaoka, Y. Mutoh, Effects of dissolved oxygen on fatigue characteristics of austenitic stainless steel in 0.9wt% sodium chloride solutions, Procedia Eng. 10 (2011) 1333–1338, https://doi.org/10.1016/j.proeng.2011.04.222.
[85] R. Francis, G. Byrne, G. Warburton, Paper No. 11351, The corrosion of superduplex stainless steel in different types of seawater. Paper presented at the Corrosion 2011, Houston, Texas, USA, March 2011.
[86] A. Al Wahaibi, T. Al Nabhani, P. R. Flores, N. Al Behalni, Paper No. 10799, Evaluation of the effect of oxygen on CRA materials. Paper presented at the Corrosion 2018, Phoenix, Arizona, USA, April 2018.
[87] B. Issa, V.Y. Bazhin, N.M. Telyakov, A.N. Telyakov, The role of chloride, oxygen and aluminum on corrosion resistance of coiled-pipes in tubular furnaces of oil refinery, in: IOP Conference Series: Materials Science and Engineering 666 (2019) 012027. https://doi.org/10.1088/1757-899X/666/1/012027.
[88] A. Meroufel, N. Larché, S. al Fozan, D. Thierry, Crevice corrosion behavior of stainless steels and nickel-based alloy in the natural seawater – Effect of crevice geometry, temperature and seawater world location, Desalination Water Treatment. 69 (2017) 202–209. https://doi.org/10.5004/dwt.2017.0448.
[89] H. Zeng, Y. Yang, M. Zeng, M. Li, Effect of dissolved oxygen on electrochemical corrosion behavior of 2205 duplex stainless steel in hot concentrated seawater, J. Mater. Sci. Technol. 66 (2021) 177–185, https://doi.org/10.1016/j.jmst.2020.06.030.
[90] R.D. Mack, J. Carminati, Paper No. 08090, Performance of selected corrosion resistant alloys under simulated seawater injection conditions downhole, NACE - International Corrosion Conference Series. (2008) 080901–080909.
[91] Y. Yang, H. Zeng, S. Xin, X. Hou, M. Li, Electrochemical corrosion behavior of 2205 duplex stainless steel in hot concentrated seawater under vacuum conditions, Corros. Sci. 165 (108383) (2020) 1–10, https://doi.org/10.1016/j.corsci.2019.108383.
[92] A.A. Dastgerdi, A. Brenna, M. Ormellese, M.P. Pedeferri, F. Bolzoni, Experimental design to study the influence of temperature pH and chloride concentration on the pitting and crevice corrosion of UNS S30403 stainless steel, Corros. Sci. 159 (2019), 108160, https://doi.org/10.1016/j.corsci.2019.108160.